Earth's sediment cycle during the Anthropocene

7 authors, including:

Juan D Restrepo
Universidad EAFIT
57 PUBLICATIONS   **1,892** CITATIONS

SEE PROFILE

Yoshiki Saito
Shimane University
339 PUBLICATIONS   **18,424** CITATIONS

SEE PROFILE

Houjie Wang
Ocean University of China
118 PUBLICATIONS   **5,254** CITATIONS

SEE PROFILE

Some of the authors of this publication are also working on these related projects:

Marine Geo-environment View project

Morfodinámica de los deltas fluviales colombianos View project

Earth's sediment cycle during the Anthropocene

Jaia Syvitski [ID][1][✉], Juan Restrepo Ángel[2], Yoshiki Saito [ID][3,4], Irina Overeem [ID][1], Charles J. Vörösmarty [ID][5], Houjie Wang[6] and Daniel Olago[7]

Abstract | The global sediment cycle is a fundamental feature of the Earth system, balancing competing factors such as orogeny, physical–chemical erosion and human action. In this Review, values of the magnitudes of several sources and sinks within the cycle are suggested, although the record remains fragmented with uncertainties. Between 1950 and 2010, humans have transformed the mobilization, transport and sequestration of sediment, to the point where human action now dominates these fluxes at the global scale. Human activities have increased fluvial sediment delivery by 215% while simultaneously decreasing the amount of fluvial sediment that reaches the ocean by 49%, and societal consumption of sediment over the same period has increased by more than 2,500%. Global warming is also substantially affecting the global sediment cycle through temperature impacts (sediment production and transport, sea ice cover, glacial ice ablation and loss of permafrost), precipitation changes, desertification and wind intensities, forest fire extent and intensity, and acceleration of sea-level rise. With progressive improvements in global digital datasets and modelling, we should be able to obtain a comprehensive picture of the impacts of human activities and climate warming.

[1]INSTAAR and CSDMS, University of Colorado, Boulder, CO, USA.

[2]Dept. Earth Sciences, EAFIT University, Medellín, Colombia.

[3]Estuary Research Center, Shimane University, Matsue, Japan.

[4]Geological Survey of Japan, AIST, Tsukuba, Japan.

[5]Environmental Sciences Initiative, Advanced Science Research Center at the CUNY Graduate Center, New York, USA.

[6]College of Marine Geosciences, Key Laboratory of Submarine Geosciences and Prospecting Technology, Ocean University of China, Qingdao, China.

[7]Institute for Climate Change and Adaptation, University of Nairobi, Nairobi, Kenya.

✉e-mail: syvitski@ colorado.edu

The global sediment cycle is a fundamental feature of the Earth system, representing the balance among factors such as mountain building, physical and chemical erosion by precipitation, biota, currents, waves or ice, and ultimately burial. Humans have collectively and substantially altered pre-industrial sedimentary stores and fluxes, with this global-scale impact arising from countless human actions, happening predominantly at very local scales but reverberating through a continuum of processes that link sediments from source areas to sequestration zones. Understanding this cycle is a central global change problem. Major factors that accelerate sediment movement off the landmass include land conversion, cropland and pasture management, construction, mining operations, and extraction of sand and gravel for building materials, each of which typically generates sediment erosion rates well above those of natural landscapes[1]. Hydraulic engineering (such as dams and reservoirs) impedes a substantial fraction of otherwise natural global sediment fluxes, and the channelization of rivers and interbasin transfers reroutes huge quantities of water and sediment. Consequently, the natural sediment cycle is currently severely imbalanced.

The imbalance arises from the intimate connection of humans with water and sediment. Managing river discharge, for example, creates opportunities to develop reliable water resources, especially in a capricious climate. However, poor water management can produce water scarcity, elevated flood potential, and altered sediment movements along river corridors, which jeopardize built infrastructure. Artificial impoundments starve downstream receiving waters of important sources of sediment, leading to unintended and dangerous erosion of sensitive sedimentary environments far from the original engineered structure[2].

Complexity is the hallmark of the global sediment system, as production and erosion processes vary spatially, across small units of landscape to entire sedimentary basins, and temporally, on timescales ranging from months to millions of years[3,4]. As a result, sedimentary system responses to human disturbance are mismatched with the sediment that is ultimately transferred to the coastlines. The system is memory-laden; for example, sediments eroded from colonial-era fields in the Piedmont in the eastern USA are transported by sequential movement through small upland streams to larger rivers, floodplains and, ultimately, artificial reservoirs[5].

The modern sediment cycle is intertwined with climate change. In the long term, the global geological cycle regulates climate and feeds back on itself, adjusting precipitation and temperature patterns or vegetative cover, all of which initiate differential erosion of the continents. Accelerated climate change from anthropogenic warming independently alters these redistribution

Key points

- Sediment production (supply) from anthropogenic soil erosion, construction activities, mineral mining, aggregate mining, and sand and gravel mining from coasts and rivers, has increased by about 467% between 1950 and 2010.
- Sediment consumption in the Anthropocene, including from reservoir sequestration, highway development and coal and concrete consumption, has increased by about 2,550% between 1950 and 2010.
- Transport of sediment from land to the coastal ocean (via rivers, wind, coastal erosion, and ice loss) has decreased by 23% between 1950 and 2010, whereas transport of fluvial particulates including organic carbon has decreased by 49% over the same period; offsets include increases in sediment delivery by icebergs and glacial melt.
- If it were not for sequestration of sediment behind dams, global rivers would have increased their particulate loads by 212% between 1950 and 2010.
- Anthropocene impacts on the marine sedimentary environment remain poorly characterized but, on the basis of the resuspension of seafloor sediment from trawling, dredging and land reclamation, anthropogenic transport seems to have increased by 780% between 1950 and 2010.
- The Earth's present Anthropocene sediment load (net land-to-sea sediment delivery and anthropogenic sediment production) exceeds 300 billion tons (Gt) per year, a mass flux that includes a small (<6%) contribution from natural processes.

Aeolian transport
Movement of detrital particles from one place to another by wind, including over mountain tops.

Endorheic
River systems that empty into receiving waters located on the continental landmass.

Exorheic
River systems that, in a particular climate, empty into coastal receiving waters.

Dissolved load
(Q_d). Portion of a stream's total sediment load derived from biogeochemical weathering of rock and soil and carried in solution by a landscape's drainage system.

Denudation rate
Sum of all processes that contribute to the lowering of Earth's terrestrial surface, including erosion.

Substrate
A layer of earth material such as soil, clay, silt, sand or gravel.

Sediment yield
(Y). The transport load normalized to drainage area and can include both the dissolved and the particulate load in units of mass per area per unit time (for example t/km² per year or g/cm² per year).

processes, through feedbacks on erosion, fluvial and aeolian transport, and flooding of coastal sites. Sediment is produced and delivered to endorheic receiving basins such as the Caspian or Aral seas, or to Earth's coastlines (exorheic drainage), which account for 87% of the landmass drainage[6].

This Review describes the modern global sediment cycle and changes to it during the Anthropocene, highlighting differences in fluxes and storage in this epoch compared with those in the Pleistocene and Holocene. The Anthropocene Working Group (AWG) defines the Anthropocene epoch as a geological time unit for potential inclusion in the Geological Time Scale, beginning in the mid-twentieth century and extended to the present; 1950 is used in this Review Article as the end date of the Holocene epoch[7–9]. We develop budgets from a broad range of primary research: field experimentation, stratigraphic analysis, observatory data, remote sensing and computer simulations. Some budget estimates are tentative and will require further research to decrease uncertainty. We highlight the unique role of modern humans in controlling sediment flux, through direct anthropogenic manipulation of sediment deposits and fluxes and more indirectly through global warming and sea level rise, which affect sediment production, transport and the position of modern depositional sites. We assess the adequacy of the data and tools currently in use, as well as new directions for fundamental and applied research in this domain.

Sediment fluxes and budgets

Sediment forms from the physical and biogeochemical weathering of Earth's superficial material and can be altered and remobilized (eroded, transported and deposited) many times before geological sequestration. Sedimentary particles range in size from boulders >3 m in diameter to small grains of gravel, sand, silt and clay <2 × 10⁻⁶ m in diameter. Particles are liberated by gravity (for example, as landslides), thermal variations and biogeochemical mediation during soil formation.

Particles are transported by water (rivers, ocean currents), wind (aeolian transport), ice (glacial flow) and through mass failures, including debris flows and turbidity currents within lakes and oceans. Weathering also generates a dissolved load, which is carried by streams and rivers and later deposited via mediation by organisms, such as carbonate reefs, siliceous sponges and diatoms, or through evaporation where saltpans form.

Sediment budgets. Within a given spatial domain, whether global, continental or catchment, the mass of eroded sediment is equal to the mass transported and deposited. Together, these terms, if complete, define the sediment budget for a domain. Here, Earth's global sediment budget is defined as the sediment mass transported from land to sea by all possible processes and measured along Earth's coastline[10–12]. This definition minimizes multiple counting of the same sediment mass in transit. In closed sedimentary systems, regional budgets are constructed from the rate that sediment accumulates across a geological interval within the receiving basins and equals the sediment flux off the landscape during the same interval.

In the past 541 million years (the Phanerozoic Eon), Earth's global deep-time denudation rate averaged 24 m per million years, a land-to-sea sediment flux of around 5 Gt per year (REF.[1]) (Supplementary Table 1). During the Quaternary period (2.58 million years ago to the present), rivers delivered about 11.4 Gt per year to coastlines, more than twice the Phanerozoic average (Supplementary Table 1), with ice sheet growth and melting the probable causes of the increased flux[13]. Continental-scale sediment fluxes (TABLE 1) reflect the geological distribution of landmass heights and their climatology. Over geological time, topography and climate will change, as will the delivery of sediment to the coastal ocean[14].

Sediment erosion and yield. Sediment erosion is the vertical loss of substrate at a specific location, in units of depth per time, with magnitudes that vary with the spatial scale. Erosion depth, when averaged over a geographic area and converted to a sediment mass, defines sediment yield, a net flux in units of mass per area per time. Sediment yields of rivers decrease as the size of the drainage area increases, with yields in larger basins reflecting sediment storage across vast lowland areas[15]. The global average sediment yield is 154 t km⁻² per year (REF.[16]). Continental sediment yields are in the range 30–1,300 t km⁻² per year (REF.[17]) (TABLE 1). Mountain belts have the highest yields[15]: Taiwan (7,800 t km⁻² per year), the Himalayas (4,800 t km⁻² per year), the Andes (1,500–5,000 t km⁻² per year), southeast insular Asia (2,300 t km⁻² per year), New Zealand (2,000 t km⁻² per year), Greenland (1,300 t km⁻² per year) and the European Alps (430 t km⁻² per year). A few low-lying regions produce large amounts of sediment, for example loess deposits with highly mobilizable substrates[18]. Subpolar and polar regions have low yields (<20 t km⁻² per year), given their frozen soils, short transport season, hard craton lithology and limited precipitation[19–21]. Regions influenced by earthquakes, often associated with plate boundaries and mountain ranges, are sediment

production hotspots[22,23]. Sediment concentrations within river water (averaged across continental regions) are in the range 110–420 g m^{−3}, although Greenland's turbid proglacial rivers and subglacial plumes might average 2,000 g m^{−3} (REF.[24]) (TABLE 1).

Some of Earth's eroded sediment is stored geologically in terrestrial 'sinks': foreland basins, fault complexes, mantle-created topography[25], basins formed from lithospheric cooling following stretching, isostatic and flexural depressions, and salt or mud tectonic zones[26,27]. Of Earth's Quaternary sedimentary volume, around 26% was stored in the landmass[10]. For example, about 14% of Rio Magdalena's suspended load is sequestered within the Mompox depression, resulting in Holocene deposits 10–130 m thick[28]. The Dong Ting depression located at the intersection of the Yangtze and Xiang rivers (China) has sequestered 128 million tons (Mt) per year since 1950 (around 7.7 Gt in 60 years)[29]. Sediment storage is also less permanent in areas that are frequently flooded, including lakes, reservoirs, alluvial fans, floodplains, avulsion zones and coastal deltas. For example, in a study of 33 major river systems, 85% experienced extensive flooding within one decade, with each flooding event adding sediment to the landscape[30]. Most eroded sediment is deposited immediately adjacent to its source[30,31]. For example, a 33% increase in soil erosion in the Colombian Andes led to only a 9% increase in river loads[32]. Most soil erosion on continental plains is caused by wind[33]. Soil erosion in the twentieth century across the conterminous USA was around 5.3 Gt per year (around 75 Gt per year worldwide; TABLE 2)[34], yet rivers in the USA transported just 0.44 Gt per year to the coastline[35].

Ocean storms are the main mechanism for eroding and transporting shoreline sediment offshore. Coastal erosion is dampened by the resupply of fluvial sediment to the shoreline. Between 1128 and 1855, the Yellow River discharged into the Yellow Sea[36] but since an avulsion in 1855 shifted the river mouth to the Bohai coast, the abandoned Yellow Sea delta has been eroding at the alarming rate of 790 Mt per year (REF.[37]). The modern Yellow Delta (Bohai Sea) is at similar risk owing to impoundment of sediment by upstream dams: 210 Mt per year of new sediment is needed to maintain the form of the delta, and twenty-first-century loads have mostly been below this value[38]. Risk of this kind is widespread, with dam-intercepted fluvial sediment an important determinant of net subsidence across many deltas worldwide[39].

Once fluvial sediment is flushed into the marine environment, local conditions determine the sediment's short-term fate. Where fluvial loads are <2 Mt per year, sediment usually accumulates within the coastal zone[40]. Where continental shelf widths are narrow (<12 km), sediment usually accumulates in nearby submarine canyons[41]. Where tidal ranges and offshore waves are small, sediment accumulates proximally[40]. Where fluvial loads are <100 Mt per year and wave heights are >2 m, distal sediment accumulation dominates. Where loads are >100 Mt per year and tidal ranges are >2 m, a subaqueous clinoform forms on the continental shelf[40].

Fluvial transport of sediment and carbon. The dominant geological pathway towards the coastal ocean is via rivers that are themselves conditioned by geomorphic and tectonic influences (drainage area, relief and basin lithology), climate and climate trends (temperature, precipitation and ice cover), and influences from a growing human population and their economic activity, including dam building, river channelization, construction, deforestation and industrial farming[7,16].

Table 1 | **Water and particulate discharge to Earth's coastal oceans during the Anthropocene**

Continent or land mass	Continental discharge		Particulate (suspended and bedload) discharge[a]			
	Drainage area (million km²)	Water discharge (km³ per year)	1950 sediment load (Gt per year)	2010 sediment load (Gt per year)	2010 concentration (g m⁻³)	2010 yield (t km⁻² per year)
Africa	20	3797	1.7	0.6	160	30
Asia	31	9806	5.5	2.4	245	77
Australasia	4	608	0.3	0.2	330	50
Europe	10	2680	0.6	0.3	110	30
Indonesia, Borneo and Papua New Guinea[b]	3	4251	2.6	1.8	420	600
North America	21	5819	1.8	0.8	140	38
South America	17	11,529	3.0	1.3	115	76
Greenland[c]	0.84	446	0.2	1.1	2470	1310
Small oceanic islands	0.01	20	0.003	0.002	100	200
Global average[d]					457	269
Global total	107	38,956	15.7	8.5		

[a]Values in the table represent continental coastline fluxes, adapted from REF.[17] with updates (see TABLE 2, Supplementary Table 4).
[b]Also includes nearby surrounding islands. [c]Greenland values are estimates for 1999–2013 (REF.[24]). [d]Area-weighted average.

Table 2 | **The Anthropocene sediment budget for Earth**

Sediment cycle component	Sediment (Gt per year)		Change (%)	Scaling notes[a]	Refs
	1950	2010			
Anthropocene terrestrial production rates					
1. Global soil erosion	25	75	200	1950: to human population	[30,34]
2. Global construction	7.5	22.5	200	1950: to human population	[1,114]
3. Mining and waste production	10	101	910	1950: to Al, Fe and Cu production	[7,105]
4. Global aggregate production	1.6	50	3,025	1950: to cement production	[7,106,107]
5. Sand and gravel mining from coasts and rivers	0.1	2	1,900	1950: to GDP; 2010: tentative	[7]
6. Total (1 + 2 + 3 + 4 + 5)	44.2	250.5	467		
Anthropocene consumption rates					
7. Global reservoir sediment sequestration	2.8	65	2221	1950: to reservoir capacity	[7]
8. Global highway sediment consumption	0.1	20	19,900	1950: to motor vehicle numbers	[7]
9. Coal consumption	0.7	5.6	700	1950: to US consumption rates	[105]
10. Global concrete consumption	0.9	28.5	3,067	As reported	[107]
11. Total	4.5	119.1	2,547		
Anthropocene land to sea flux					
12. Global fluvial suspended load (Q_s)	14.5 ± 1.5	7.2 ± 0.9	−50	2010: to observations in Supplementary Table 4	REF.[17], this study
13. Global fluvial bedload (Q_b)	1 ± 0.4	0.3 ± 0.2	−70	1950 and 2010: scaled on Q_s and river mining	REF.[17], this study
14. Global fluvial dissolved load (Q_d)	3.9	3.6	−7.3	1950: REF.[69]; 2010: see Supplementary Tables 3 and 4	[91]
Global dissolved silica	0.42 ± 0.07	0.42 ± 0.07	?	Interval difference study needed	[88]
Global dissolved organic carbon	0.21	0.21	?	Interval difference study needed	[50]
Global dissolved inorganic carbon	0.38	0.38	?	Interval difference study needed	[50]
15. Global particulate organic carbon	<0.24	<0.24	?	Interval difference study needed	[51]
16. Global aeolian land-to-sea flux (Q_a)	1.5	1.5	?	Interval difference study needed	[21,92,93]
17. Global coastal erosion flux (Q_c)	0.5	>0.5	?	Updated compilation needed	[10]
18. Glacial meltwater flux (Q_m)	0.2	1	400	1950: to glacial ice loss	[24,164]
19. Global iceberg sediment flux (Q_i)	0.6	3	400	1950: to glacial ice loss	[24,164]
20. Total (12 + 13 + 14 + 15 + 16 + 17 + 18 + 19)	22.4	17.3	−23	River fluxes offset by ice ablation	
Potential fluvial particulate load					
21. Reservoir deposits likely to have reached the coastal ocean	2.1	48	2,186	1950: to reservoir capacity	REF.[10], this study
22. Total (12 + 13 + 15 + 21)	17.8	55.7	212		

Table 2 (cont.) | **The Anthropocene sediment budget for Earth**

Sediment cycle component	Sediment (Gt per year)		Change (%)	Scaling notes[a]	Refs
	1950	2010			
Anthropocene alteration to marine sediment					
23. Global trawling resuspension transport	2.9	22	659	1950: to fishing vessel power	[150,234]
24. Dredging and land reclamation	0.7	9.8	1,300	As reported	[105]
25. Total (23 + 24)	3.6	31.8	783		
Anthropocene total load (6 + 20 + 25)	70.2	299.6	327		

[a]Values for 1950 represent rates for mid-twentieth century. See Supplementary Box 1 for further details about scaling.

A river's suspended load might vary by an order of magnitude or more across a flood event or seasons, or with changes in water sources or in land-use and landcover processes that supply sediment to river networks[42]. Most rivers carry their annual load within a single season[43], for example, monsoonal systems such as the Ganges and Brahmaputra rivers[44], or Arctic rivers[45,46]. Small flashy rivers such as the Eel River in California carry 90% of their annual sediment load within a few weeks[47]. Continent-spanning rivers distribute their carrying capacity over longer intervals; for example, the Mississippi River takes 7.5 months to carry 90% of its annual load[48], whereas the Congo River takes 9 months[49].

The fluvial transport of particulate organic carbon (POC) is closely linked to the concentration of suspended sediment[26]. Globally, rivers export 0.21 Gt per year of dissolved organic carbon, 0.38 Gt per year of dissolved inorganic carbon[50] and about 0.24 Gt per year of POC[51] to the ocean (TABLE 2). Global estimates are compiled from regional relationships between sediment concentration and organic carbon[51]. Particulate nitrogen and particulate phosphorus are in turn positively correlated with particulate carbon concentrations[52]. The coastal margin is the major hotspot for organic carbon burial[53]. River delta and non-deltaic shelf regions bury an estimated 0.11 Gt C per year and 0.07 Gt C per year, respectively, whereas only about 0.006 Gt C per year is buried in the open ocean[54]. The burial efficiency of terrestrial POC (around 36%) is much higher than that of POC originating from marine primary production (0.25%)[54]; therefore, land-to-ocean export of POC is an effective carbon sink[55]. POC from subtropical regions accounts for much of the global delivery to oceans[56,57] but is accompanied by the release of CO_2 and methane[58].

Plastic is becoming an ever-increasing component of sediment transport, as plastic production increased from around 2 Mt per year in the 1950s to 359 Mt per year in 2018 (REFS[59,60]). Plastic debris enters the ocean at a rate of 4.8–12.7 Mt per year (REF.[61]), and microplastics are globally transported by aeolian vectors, even to Arctic snowfields[62].

River discharge and climate oscillations[63,64] or events[65] are strongly coupled. The five largest rivers in east and southeast Asia (the Yellow, Yangtze, Pearl, Red and Mekong rivers) display short-term (interannual-scale) variation in sediment flux, dominated by natural climatic oscillations such as the El Niño–Southern Oscillation (ENSO)[66]. All South American rivers, independent of size, display a strong seasonal variability in discharge and sediment load, typically a 5–10-fold difference between low and high monthly discharges. The interannual variation of discharge and sediment load associated with ENSO can be almost as great, typically a 2–4-fold difference between low and high annual discharges[67,68]. In the Magdalena River, variations in the Southern Oscillation Index (SOI) explain 54% of the variability in sediment load[69]. Further analysis of the Oceanic Niño Index (ONI) reveal that sediment load increased during 10 of 13 La Niña events between 1972 and 2011 (REF.[32]).

Quaternary sediment budget. Of the approximately 43 Pt of Earth's Quaternary sediment mass, 74% is marine-based and largely off the continental shelves, and 26% is continental, of which 85% is siliciclastic and 15% is largely of carbonate material[10]. During the Pleistocene Epoch, Earth's land area expanded by around 16 million km[2] as sea level fell and when many rivers discharged their loads directly into the deep ocean[70]. For example, 95% of siliciclastic sediment was transported beyond the shelf edge off New Jersey during the Quaternary[71]. Waxing Pleistocene ice sheets and their ice streams also delivered more sediment directly to the deeper ocean than earlier in the Cenozoic era[72,73]. After global sea level stabilized at around 6,700 years before present and across the Meghalayan Age (FIG. 1), ever more Holocene sediment was sequestered, either terrestrially in deltas or offshore, largely on continental shelves[74]. Given the Quaternary sediment mass of around 43 Pt within a 1.8-million-year interval, of which 74% would have reached the coastal ocean[10], the Quaternary sediment flux off of the global landscape is around 17.8 Gt per year, of which 64% is carried by rivers (Supplementary Table 1).

Holocene sediment budget. No study has yet offered a global sediment budget for the Holocene epoch (11,700 years before present to 1950). Obtaining an estimate would be a considerable undertaking, given the substantial variation in sea levels and fluvial loads over this period and time-dependent and delayed responses to changes in climate, deglaciation and the impacts of humans on the landscape during the recent Meghalayan Age (Supplementary Table 1). For example, during the deglacial period (21,000–10,000 years before present),
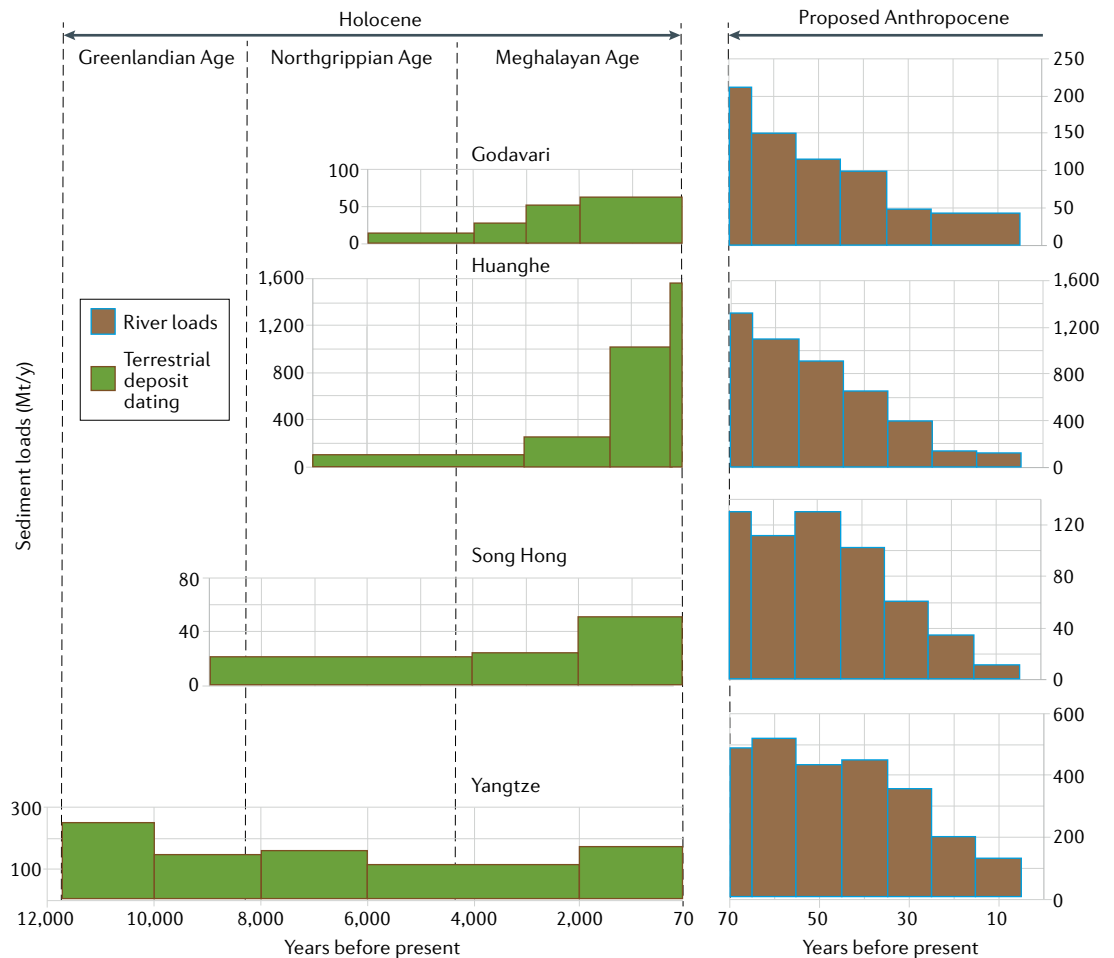
Fig. 1 | **Examples of fluvial sediment loads in the Holocene and Anthropocene.** The bar graphs depict the sediment loads for four medium-to-large Asian rivers: the Godavari River (India)[234,235], the Huanghe (or Yellow) River (China)[80,81], the Song Hong (or Red) River (Vietnam)[236] and the Yangtze River (China)[77]. Records are of unequal duration and intervals. Holocene estimates of sediment discharge are based on terrestrial coring, dating and deposit mapping and offshore sediment dispersal patterns. The trapping efficiency of deltas is about 70% for the Yangtze, 70–80% for the Huanghe, and unknown for the Song Hong and Godavari deltas. Reconstruction for the entire Holocene Epoch (green) is only possible for the Yangtze River. Estimates for the Anthropocene epoch (brown), corresponding to 1950 to the present, are based on the river load entering a delta.

Greenlandian Age
The earliest age of the Holocene Epoch, extending from 11,700 years to 8,236 years before the year 2000. Also known as the early Holocene. The Northgrippian Age (the middle age of the Holocene Epoch and thus also known as the middle Holocene) extends from 8,236 years to 4,250 years before the year 2000.

the Po River delivered a 75% larger load than in the post-glacial Holocene (<10,000 years before present)[75]. In the period 11,000–7,000 years before present, the Ganges and Brahmaputra rivers delivered 2.3 Gt per year of sediment, more than double the twentieth-century loads of about 1 Gt per year (REF.[76]); the Yangtze River loads have a similar ratio[77]. For many coastal settings, older (Greenlandian Age) terrestrial deposits remain poorly studied, as they were buried by prograding mid-to-late-Holocene (Meghalayan Age) deltaic deposits (FIG. 1). The tentative estimate for land-to-sea flux in the Holocene deglacial interval is around 22 Gt per year, which is higher than the post-glacial Holocene rate of around 11 Gt per year. However, both estimates need to be refined, which will require a community effort.

Human-caused erosion can be detected across thousands of years[78,79] and is driven mainly by regional deforestation for agriculture[78]. These signals manifest in a few coastal settings, such as the Godavari delta, where a subdued preindustrial anthropogenic signature

is detected (FIG. 1). Both the Yellow and Yangtze rivers carried increased loads for about 2,000 years before present owing to deforestation[80], and in the case of the Yellow River, through an easily disturbed loess landscape[81] (FIG. 1). However, recent afforestation and soil conservation practices have contributed to decreased loads in these river systems[77,82]. In general, onset of the human footprint is globally diachronous, as it is catchment-unique and tied to spatial patterns of human action. For example, sediment loads of the Waipaoa River in New Zealand increased by 140% after the arrival of the Polynesians around 1300, 350% after European colonization around 1800 and 660% after catchment deforestation in 1900 (REF.[83]). Climate–vegetation feedbacks have also influenced terrestrial sediment yields: sediment discharge off the Indian subcontinent increased when the wet middle-Holocene conditions were replaced by drier savannah conditions of the late Holocene, and where vegetation changed from C3 plants to C4 grassland plants[84].

Bedload
(Q_b). Grains rolling, sliding or bouncing along a river channel or desert surface. Bedload dominates river transport in mountain regions or other steeper regions of the landscape that are being eroded.

Anthropocene sediment budget. Natural processes are responsible for transporting approximately 22.4 Gt per year of sediment to Earth's global ocean since 1950, although with a strong anthropogenic signal, and thus at a higher rate than for the Quaternary average (TABLE 2; FIG. 1; Supplementary Table 1). Sediment transport by natural processes has since fallen to about 7.3 Gt per year in 2010, largely owing to sequestration of sediment behind dams[2,85] (TABLE 2; FIG. 2; Supplementary Tables 2–4).

Earth's dissolved silica budget[86,87] offers a useful example of the many different elemental dissolved loads and how they differ from the particulate budget. Silica enters Earth's oceans[88] at 14.8 ± 2.6 Tmol per year (416 ± 73 Mt per year) via rivers (about 227 Mt per year), groundwater (about 65 Mt per year), seafloor weathering (about 53 Mt per year), hydrothermal sources (about 48 Mt per year), aeolian transport (about 14 Mt per year) and polar and subpolar glaciers (about 8 Mt per year). Sequestration of silica[88] occurs at 438 ± 67 Mt per year, including diatom burial (about 258 Mt per year), reverse-weathering reactions (about 132 Mt per year) and utilization by siliceous sponges on continental shelves (about 48 Mt per year). Dissolved silica within Earth's oceans is recycled approximately 16 times before sequestration, providing a geological marine residence time of around 8,000 years[88]. By contrast, in the terrestrial domain, multiple opportunities for particulate recycling are present across large continental-scale basins, whereas short and mountainous river basins offer little potential[89]. In the marine environment, seafloor sediment might experience multiple 'cycling' events before burial on continental margins or abyssal plains. In shallow coastal waters, particles might undergo resuspension and burial hundreds of times through the action of waves or tides before final marine burial[90].

Worldwide, about 10,500 rivers and streams have a drainage area >50 km² and a discharge >1 m³/s but most of the water and sediment is delivered by a subset comprising about 1,100 rivers delivering 90% of terrestrial runoff, and about 450 rivers transporting 90% of the global fluvial load (TABLE 2; Supplementary Table 2; Supplementary Figure 1). Particulate transport by rivers is divided between suspended load (about 93% on average), bedload (about 6% on average) and organic carbon (about 1.5% on average), and was delivered at a rate of around 15.7 ± 1.5 Gt per year in 1950 and 7.7 ± 0.9 Gt per year in 2010 (TABLE 2). During the same interval,
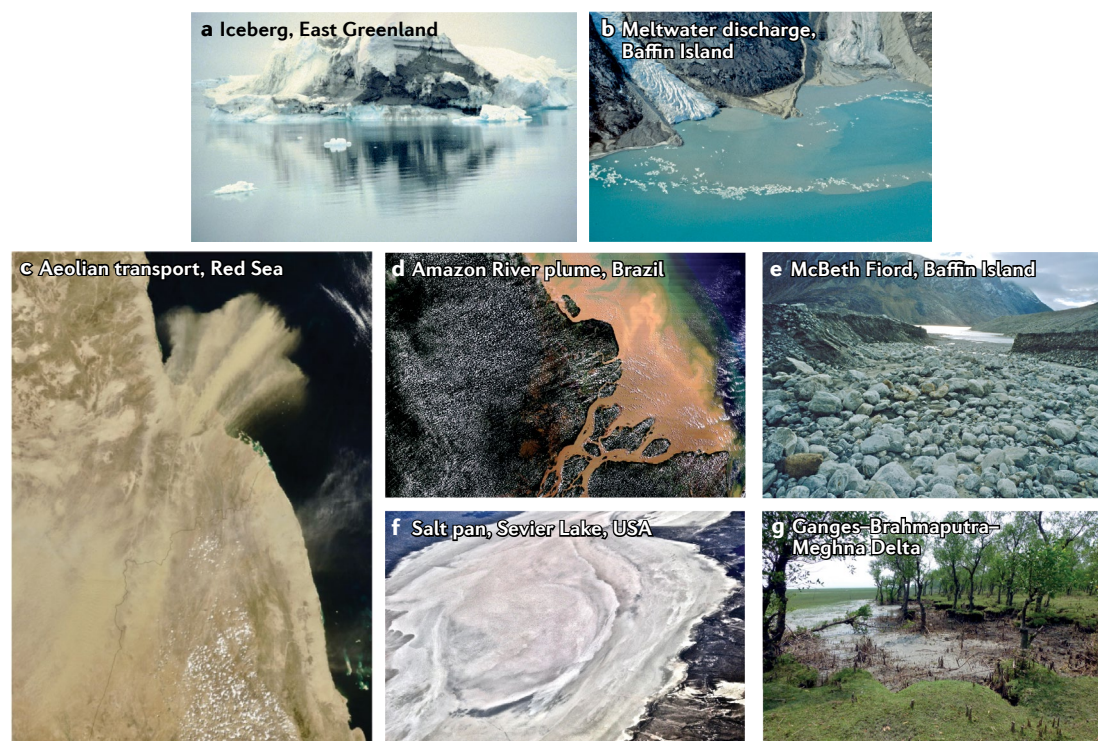

Fig. 2 | **Examples of geological categories of sediment delivery to the global ocean.** Human action has altered transport vectors, either through global warming impacts or globally manifested anthropogenic alterations to the natural environment. **a,b** | With global warming, iceberg production and rafting of sediment (part **a**) has increased substantively over the past 70 years, in tandem with the production of meltwater discharged into the coastal ocean (part **b**). **c** | Red Sea satellite image showing aeolian transport of sediment across the coastal ocean; workflows are needed to recover historical trends. **d,e** | Examples of fluvial loads of sediment from Brazil (part **d**; suspended load in a plume of the Amazon River) and Baffin Island (part **e**; bedload lag in McBeth Fiord), are decreasing globally for multiple reasons, particularly river damming and riverbed mining. **f** | Saltpans, such as Seviers Lake, store the dissolved load from their endorheic drainage. Global historical trends are poorly known for exorheic drainage. **g** | Sediment removed by coastal erosion, such as along the Ganges–Brahmaputra–Meghna Delta (Bangladesh and West Bengal, India), remains poorly constrained. Further details about sediment delivery are available in TABLE 2. Part **c**, image courtesy of Jeff Schmaltz, MODIS Rapid Response Team, NASA/GSFC. Part **d**, image courtesy of MODIS Rapid Response Team, NASA/GSFC. Part **g**, image courtesy of Kimberly Rogers.

the dissolved load sourced from rock and soil decreased from around 3.9 Gt per year in 1950 (REF.[91]) to 3.6 Gt per year in 2010, as a result of reduced freshwater runoff reaching the coastal ocean (TABLE 2).

Wind carries approximately 1.5 Gt per year to the ocean, which is only a small fraction of the total terrestrial aeolian flux[21,92,93]. Increased global observations and modelling efforts are needed to determine whether aeolian global fluxes have altered during the Anthropocene epoch. Coastal erosion is largely through the action of waves and tides, resulting in a delivery rate of about 0.5 Gt per year (REF.[10]) that has probably increased with rising sea levels, loss of wetlands and mangroves, and reduction in sediment supply[94]. Ice sheets and their glaciers delivered 0.8 Gt per year of sediment to the ocean in 1950 (TABLE 2), a rate that increased to around 4 Gt per year in 2010 (TABLE 2), about 25% as subglacial meltwater and about 75% from the calving and melting of icebergs[24].

Human activities alter sediment fluxes

Human action can simultaneously increase and decrease the natural cycle of sediment transfer to the coastal ocean depending on where the action occurs within the landscape[2], including impacts on a broad range of weathering products[85]. Increases in a river's sediment load reflect large-scale landscape disturbances, including deforestation (for example, the Araguaia River, Brazil)[95], conversion of pastureland to cropland (the Magdalena River, Colombia)[96], intensification of farming in erosive substrate (the Yellow River, China)[36,97,98], industrial farming (the Mississippi River, USA)[17], road construction (the Lanyang River, Taiwan)[99] and mining (the Kolyma River, Russia)[100]. Decreases arise from soil conservation (the Yellow River, China)[100,101], riverbank hardening (the Rhine, Germany)[17], dam construction (the Nile, Egypt and Sudan)[102], channel-bed mining (the Mekong River, east and southeast Asia)[103] and waterway diversions (the Indus River, Pakistan)[104]. There is often a sequence to these human interventions, first to increase river loads (for example, from deforestation and industrial agriculture), then to decrease loads (for example, by river damming)[17].

Even by 1950, sediment production (supply) from human action was substantive (44.2 Gt per year), almost double the 22.4 Gt per year from all-natural transport mechanisms (TABLE 2). The largest source from human action was soil erosion from deforestation and agriculture (25 Gt per year), followed by mining and waste production (10 Gt per year), construction (7.5 Gt per year), aggregate production (1.6 Gt per year), and sand and gravel mining from coasts and rivers (0.1 Gt per year). By 2010, sediment production from human action increased by 467% to 250.5 Gt per year, with mining and associated waste production at present exceeding that from soil erosion (TABLE 2). Mining has changed the global landscape (FIG. 3), with millions of abandoned mines, or mountain tops removed to access coal deposits, concomitant with dumping of spoils[7] (FIG. 3c,d). Global coal production and associated waste is at present about 74 Gt per year (REF.[105]); other mineral extraction including overburden and waste removal contributes

around 28.5 Gt per year (REF.[105]). Global aggregate production is about 50 Gt per year (REF.[106]) and sand and gravel mining of riverbeds and beaches produces an estimated 2 Gt per year (TABLE 2; FIG. 3).

Anthropocene sediment consumption rates rose from 4.5 Gt per year to 119.5 Gt per year (a 2,550% increase) between 1950 and 2010 (TABLE 2). Sediment is redistributed to construct global highways and railways, buildings and other infrastructure, or is converted into concrete, the most abundant anthropogenic rock[107]. In 2019, coal consumption was 8.6 Gt per year. Sediment that is impounded behind dams (65 Gt per year at present) is considered to be consumed unless subsequently released (TABLE 2).

Deforestation, agriculture and soil erosion. In North America, continent-wide rates of sediment accumulation have been broadly stable for the past 40,000 years or so, with accumulation balanced by erosion[108]. Soil erosion increased 10-fold when agricultural land in North America expanded from <0.1 million km^2 in 1820 to 5.2 million km^2 at its peak in 1950, similar in timing to the history of river modifications associated with European colonization[108,109]. Soil loss from agricultural land in the USA is currently 2.8–4.2 Gt per year, a surface loss of around 0.5–0.7 mm per year, which is well above natural rates of 0.01–0.04 mm per year (REFS[110,111]) and similar to the global average[112].

For most rivers, the anthropogenic footprint increased sharply after World War II[100], when humans broadly and globally changed the landcover[112,113] and coastal delivery rates increased by 2.3 ± 0.6 Gt per year[2]. Industrial-scale agriculture accounts for 50% of terrestrial soil loss[109]. Forest clearing for the creation of agricultural land has long increased soil erosion rates[66], but contemporary rates of soil loss from cropland on a per area basis exceed the natural rates of erosion by 30-fold[114]. Cropland represents about 11% of global land area but accounts for about 50% of soil erosion;[30] soil erosion rates from forests are 77 times lower. Of the 2.3 million km^2 of forest that was lost between 2001 and 2012, only 4% was converted to cropland but this area was responsible for over half of the increase in soil erosion[115].

The Araguaia River biome of central Brazil lost 1.2 million km^2 of Cerrado forests to agriculture in the period 1970–2000. No other biome in the world has been destroyed as quickly in human history. A total of 232 Mt of eroded sediment was stored in the main Araguaia channel and floodplain; bedload transport increased by 31% in the period 1970–2000 (REF.[95]). Deforestation of highlands creates even higher fluvial sediment loads[100,116,117]. In the Magdalena basin in Colombia, sediment transport increased by 9% (44 Mt per year)[32] owing to loss of 40% of highland forest, a 65% increase of cropland and pastureland, poor soil conservation, mining and urbanization[96]. The consequences of these activities include increased soil erosion (33% between 1972 and 2010), reduced soil productivity, compromised freshwater ecosystem services and geomorphic and ecological changes in its floodplains. Most (79%) of the Magdalena catchment remains under severe
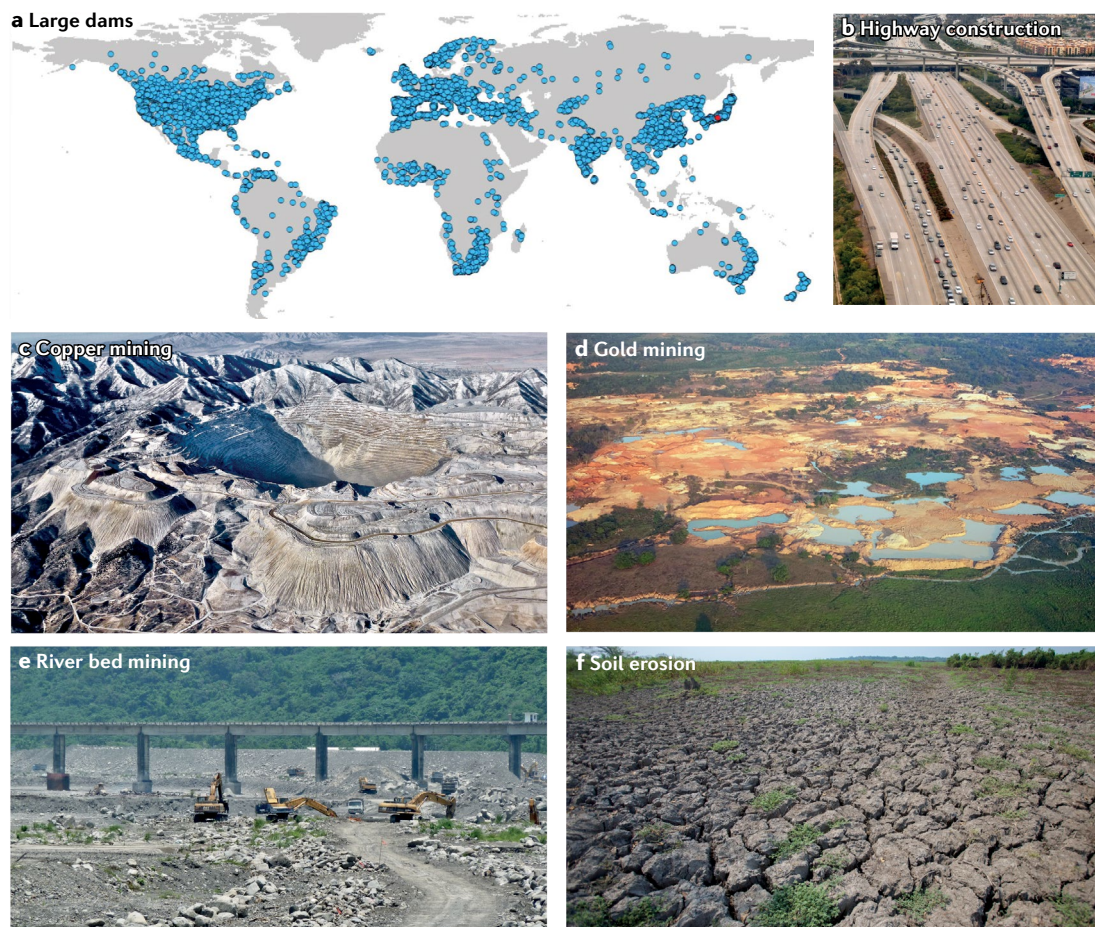
Fig. 3 | **Human action dominates the global sediment budget.** Large quantities of sediment are now generated or trapped across the terrestrial landscape by human activities. The human footprint has greatly increased in the 60-year interval from 1950 to 2010. **a** | Global distribution of large dams (>15 m in vertical height) in 2009 according to the International Commission on Large Dams (ICOLD)[122]. These dams sequester large quantities of sediment, preventing their transport downstream (including to oceans). **b** | A freeway in Los Angeles (CA, USA) exemplifies sediment sequestration in large-scale concrete construction projects. **c–e** | Sediment production has increased with the growth of mining operations, such as copper mining (part **c**, Bingham Canyon Copper Mine in Utah, USA), gold mining (part **d**, an illegal gold mine in the northern Andes, Colombia) and sand and gravel mining (part **e**, river bed mining in a Taiwanese river). **f** | Deforestation and desertification in the American tropics has increased sediment loss from loss of ground cover and erosion.

erosional conditions, owing in part to the clearance of more than 70% of natural forest between 1980 and 2010 (REF.[32]), resulting in the production of 482 Mt of extra sediments between 1972 and 2010.

River engineering and dams. Humans have inadvertently altered one of Earth's largest 'systems', global river flow, which is essential to continental sediment flux[118–120]. Today, owing to artificial impoundments and diversions, only 23% of rivers longer than 1000 km flow uninterrupted to the coastal ocean (10.5% in Europe, 18.7% in North America)[120]. At least 3,700 large dams (≥15 m in vertical storage height), either planned or under construction, will reduce the number of free-flowing large rivers remaining by a further 21% or so[121]. More than 40% of river flow is intercepted by large reservoirs[118]. Large dams are the main cause of sediment sequestration: of the 58,519 large dams registered[122], only 1.4% were built before 1850 (6.1 km³ capacity) whereas 10% were built between 1850 and 1950 (685 km³ capacity).

95.7% of the world's total reservoir capacity (>15,000 km³) was constructed after 1950. The global sediment trapping efficiency of reservoirs rose from 5% in 1950 to 30% in 1985 (REF.[118]). Large dams have trapped about 3,200 Gt of sediment since 1950 (REF.[123]), approximately 74% of which would likely have reached the coastal ocean[10]. The 'potential' fluvial particulate load then combines the observed fluvial loads with this potential reservoir load (TABLE 2), such that the potential fluvial load in 1950 was around 17.8 Gt per year (and close to background Quaternary rates; Supplementary Table 1) and 55.5 Gt per year by 2010 (TABLE 2). If it were not for dams, sediment would pour into coastal deltas.

Over the past 60 years, the sediment load of the nine major rivers in China decreased by 85% (REF.[80]). Sediment discharge into the marginal seas surrounding China decreased from 1.95 Gt per year for 1954–1968 to 1.40 Gt per year for 1969–1985, 890 Mt per year for 1986–1998, 450 Mt per year for 1999–2003, and 310 Mt per year for 2004–2015 (REF.[80]). Between 1954

Particulate load
(Q_p). Detrital particles in transit, transported by water or wind as bedload (Q_b) and suspended load (Q_s), where $Q_p = Q_b + Q_s$.

and 2015, about 71 Gt was delivered to the coastal ocean and about 53 Gt of sediment was retained on the mainland owing to reservoir trapping (45.5%), water resource utilization (29%), and soil conservation measures (25.5%)[80]. The Po River (Italy) carried 16 Mt per year of sediment in the 1930s, 12 Mt per year in the 1970s and 5 Mt per year in the 1980s, all during a time when the Po's water discharge increased[124,125]. With flood controls, distributary channels in the Po delta trap 16% of the annual load and are being super-elevated at rates of 4–10 cm per year with respect to the delta plain[124,125]. The Indus River (Pakistan) reflects a 200-year history of major river modifications:[126] artificial flood levées (stop banks), barrages and irrigation canals, sediment impoundment behind reservoirs, and inter-basin water transfers. The Indus River once transported >270 Mt per year of sediment to its delta but now delivers around 13 Mt per year, often running dry owing to water removal for agricultural irrigation. Even during floods, only a fraction of the discharge makes it to the ocean (43% in 2010)[104]. A river's dissolved load might also be affected by anthropogenic disturbances[86,127], as reservoirs starve downstream areas through water storage and dissolved load sequestration dynamics.

Engineering is used to straighten rivers, both for safety reasons and to speed up the transit time for ships sailing around large meanders. For example, the main channel of the Mississippi River was shortened by 230 km (REF.[128]), reducing transit time by about a day. River shortening increases a river's hydraulic gradient and thus bed material load. In North America and Europe, artificial levées blocking the connection of rivers to their floodplains are being removed at strategic locations[129]. In the Mississippi Delta, controlled flooding is being undertaken to restore the sediment flux needed for landform stability of coastal wetlands[130]. Between 850 BCE and 1839 CE, as the Yellow River increased its sediment load by fourfold (FIG. 2), levée breaches increased 100-fold, and breach outflow increased 27 times[98]. Between 1550 and 1855, artificial levées along the Old Yellow River suffered 313 breaches in response to the annual flood-wave, reducing channel capacity from super-elevation of its channel floor and damaging prior levée repairs[36]. Between 1580 and 1849, 78 Gt of the Yellow River's load was deposited on floodplains, with a similar mass deposited between the artificial levées[98].

Water diversion schemes are also proliferating, for example the South–North Water Transfer Project of China, often to expand agricultural production and address water scarcity[126]. Another example is India's National River Linking Project (NRLP) that will connect 44 rivers via 9,600 km of canals. One analysis forecasts a reduction in the suspended sediment transport to affected NRLP rivers: the Mahanadi River by 40–85%, the Godavari River by 71–99%, the Krishna River by 60–97%, the Ganges River by 39–75% and the Brahmaputra River by 9–25% (REF.[131]). Aggradation rates on downstream deltas are projected to decrease substantially. By contrast, redirected fluvial sediment will be stored within agricultural land, temporary storage basins and the diversion channels themselves.

Hydraulic gradient
The change in the hydraulic head over a distance along the direction of flow path. The hydraulic gradient represents the driving force that causes water to flow in the direction of maximum decreasing total head.

Bed material load
(Q_{bm}). Sediment grains that line the bed of a river or desert surface and with sufficient flow speed can be transported with the current, and consists of bedload and suspended bed material grains. $Q_{bm} = Q_b + Q_{sbm}$.

Global consumption of sand and gravel. The need for sand and gravel for engineering coastlines, road construction and building Anthropocene megacities (>10 million people) is now outstripping supply. Highway development and concrete production are major consumers. The 64 million km of global roads and highways have consumed about 200 Gt of sand and gravel[7]. In 1950, global concrete production consumed around 0.9 Gt per year of sand and gravel, and at present exceeds 27–30 Gt per year (REFS[7,132]). For concrete production, fluvial sand, being more angular, is preferred over rounded particles from coastal beaches or desert dunes. Determining the amounts of sand and gravel (and pebbles, cobbles and boulders) that are mined from Earth's global coasts and rivers remains difficult, but every continent on Earth except Antarctica offers examples. Ten sand-producing countries collectively mined 420 Mt in 2019 (USGS resource database)[133]. Illegal mining of riverbeds contributes both to uncertainties and underreporting, and is known to occur in Europe, Africa, Australia, South America, North America and Asia[133,134]. In the state of São Paulo in Brazil, illegal mines outnumber legal mines[135]. Illegal sand extraction is characterized by large, violent black markets[136,137], such as the sand mafias in Kashmir and India[138]. The best global rate estimate for this sediment resource is 0.1 Gt per year in 1950 and 2 Gt per year in 2010 (TABLE 2).

Riverbed mining greatly reduces fluvial bed-material transport. For example, the approximately 100 Mt per year of aggregates extracted from the lower and middle Mekong River[139,140] is an order of magnitude greater than the down-river transport of sand (6.2 Mt per year), resulting in riverbank and coastal erosion[141]. These trends will affect rivers for decades. Between 2000 and 2016, Singapore imported large quantities of sand of unknown provenance from Vietnam (74 Mt)[142] and Cambodia (80 Mt)[103,143]. Marine aggregates are also mined in tidal channels of China, the Republic of Korea and areas around Hong Kong and Singapore[144]. The Dongjiang River (a tributary of the Pearl River, China) contributed 272 Mt per year between 1980 and 2002 (REF.[145]). In Europe, offshore sand and gravel mining is an established industry in Denmark, France, Germany, the Netherlands and the UK. Since 1995, approximately 100 Mt per year has been extracted from the seabed of the northeast Atlantic[146].

Offshore trawling. Twenty-four continental shelves and slopes were examined for their trawling footprint, to water depths <1 km and for ≥2 years[147]. Regions varied markedly in trawling intensity, and 1.1 million km² of continental shelf was found to be trawled[147]. Trawled areas experienced widespread erosion and alteration to the physical properties of the seabed, including sediment mixing, grain-size sorting and organic carbon impoverishment[148]. In the upper portions of Mediterranean submarine canyons, sedimentation rates increased 3–4-fold since the advent of industrial-scale trawling in the 1960s[149]. The amount of seabed resuspended by bottom-trawling on Earth's continental shelves was about 22 Gt per year (REF.[150]) in 2010, more than 650% higher than in 1950 (TABLE 2).
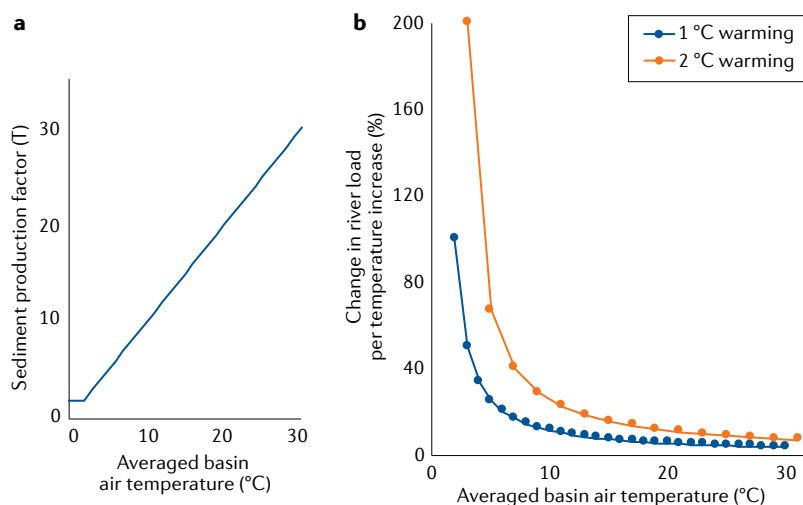
Fig. 4 | **Predicted impact of climate warming on fluvial sediment budgets. a** | Increase in fluvial sediment load with basin temperature. Warm drainage basins make more sediment available for transport by river networks (according to the BQART model). **b** | Model-predicted impact of climate warming on sediment transport. As the climate warms by 1–2 °C, the amount of sediment delivered to river systems is predicted to increase, with the greatest impact on subpolar (Arctic) environments. Cold regions emit less longwave radiation, and thus warm faster, owing to Planck feedback, than warm regions[237]. High mountain cold regions show similar trends.

Anthropogenic climate warming

Driven by the accelerated burning of hydrocarbon fuels, atmospheric temperatures have increased by 1.1 °C since 1900 (REFS[151,152]), in response to increases in greenhouse gases (H_2O, CO_2, CH_4 and N_2O)[153]. Since 1871, Earth's oceans have stored about 436 ZJ of extra solar energy resulting from the greenhouse effect[154], an order-of-magnitude more energy than is associated with direct human production and consumption[7]. Planetwide responses to atmospheric warming includes increases in ocean and land temperatures, thaw of permafrost, sea-ice loss, glacial-ice mass loss, acceleration of sea-level rise, and intensification of the global hydrological cycle.

Temperature impacts on sediment production. Drainage-basin temperature influences soil formation, soil erosion processes and climate feedbacks. Polar and subpolar regions are characterized by frozen environments that lock in otherwise mobile sediment (permafrost and frozen riverbeds), low-intensity rainfall across a short transport season, slow to no soil formation, with partly frozen coastal seas limiting coastal erosion, resulting in a reduction in sediment production and transport[21]. Temperate environments offer increased soil formation, a vegetation cover with strong root systems, increased freeze–thaw cycling[155], convective rainfall, and high levels of coastal erosion[21]. Subtropical and tropical regions receive extremes in convective rainfall onto landscapes with reduced plant-root structure and high biogeochemical weathering that releases high volumes of dissolved matter;[21] desertification and soil loss are regional phenomena[156]. Warmer basins yield more sediment to river networks, generating increased fluvial loads[16] (FIG. 4a). Large Arctic river basins capture huge regions of permafrost that have disproportionally low

sediment loads[19,20]. With climate warming, polar, subpolar and alpine regions become hotspots for increased river loads (FIG. 4b). Thawing of vast regions of permafrost will provide new sources of sediment to river systems by thaw slumping, or development of a network of thermokarst channels[157,158]. For every 2 °C increase in mean annual air temperature of Arctic basins, river sediment loads might increase by around 30%, as new sediment is liberated during thawing from their frozen state[159]. Four of the world's largest rivers and hundreds of smaller subpolar rivers are being affected by global warming. High elevation mountain environments are similarly experiencing accelerated warming and sediment production; for example, in the high mountains of Asia, a 1 °C increase has resulted in a 24% increase in fluvial sediment load[160].

Temperature impacts on the cryosphere. Summer freezing lines are rising in response to global warming, leading to more permanent adjustments to a glacier's Equilibrium Line Altitude, below which meltwater is released, along with increased levels of sediment[161]. Glaciated basins already carry increased sediment loads in comparison to non-glaciated terrain[13], and additional meltwater will enlarge these loads. Meltwater runoff averaged across 1999–2013 is at present around 40% higher than for the averaged 1961–1990 climate normal[162]. Greenland's current sediment delivery to the coastal ocean is around 56% higher than just 30 years ago[24], which is further confirmed by the accelerated progradation of Greenlandic deltas over the past three decades[163]. Estimates for 160 proglacial rivers across Greenland reveal that these rivers represent 1.1% of the global terrestrial freshwater flux and about 8% (0.9–1.3 Gt per year) of the modern suspended sediment delivery to the global ocean[24]. Rivers that originate from fast-moving glaciers become sediment-export hotspots, with 15% of Greenland's rivers transporting 80% of the ice-sheet sediment load[163].

As Earth warms, ice flow and melt will accelerate, greatly increasing sediment delivery. The global mass loss of glacial ice is now >750 Gt per year (REFS[164,165]). Greenland delivers more freshwater to the coastal ocean as icebergs (66%) than as meltwater (34%)[164]. Sediment delivery to the Greenland coastal ocean from icebergs may be as high as 2.9 Gt per year (about 4 Gt per year globally), mostly from debris-rich basal ice[24] (FIG. 1). As the Earth heats up, iceberg production will initially increase but will then decline in the more distant future as ever more ice sheet termini become land-based.

Permafrost thawing due to warming is especially important because of its impact on the global carbon cycle. Northern Hemisphere soils store about 60% of the global soil carbon[166]. Decomposition of this frozen carbon stock with permafrost thaw might represent a large new source of greenhouse gas emission[167–169]. Mobilization of this soil material is being observed[168,170] through thaw slumps and detachment slides, collapse-scar wetlands and riverbanks, but the implications for organic carbon flux delivery to the Arctic coast is not yet constrained.

In the Arctic Ocean, sea ice has diminished by 300 ± 100 km³ per year (about 275 Gt per year) since 1980

Climate normal
A 30-year interval designed to capture the variability in the climate system at a given location.

(REF.[171]). In the same time period, coastal erosion has increased, forced by an expanded fetch (wave-generating distance), increased open-water season (earlier start, later end), warmer nearshore water, and more frequent and intense storms[172,173]. Along sections of the northern Alaskan coast, erosion has increased from shoreline retreat rates of 6.8 m per year for 1955–1979, to 8.7 m per year for 1979–2002 and 13.6 m per year for 2002–2007 (REFS[174,175]). Other areas have similarly high coastal erosion rates, and more gradual erosion is dominant along the entire Arctic Ocean coast[176]. Most of the increase in erosion rates of permafrost coasts is explained by an increase in open-water duration[172], followed by increases in the magnitude and frequency of positive setup events, and coastal water temperatures[177,178].

Temperature impacts on sediment transport. Parameters affecting river temperatures include air temperature, dew point temperature, wind velocity, insolation, and the thermal flux from upstream runoff[179]. River water can be cooler or warmer than the air temperature[179]. Sediment transport is affected by changes in fluid temperature through fluid density (thermal impact range 3.5%) and kinematic viscosity (global range 72.5%), such that grain-settling velocities can vary by >90% along a single river. Resistance to grain settling is higher in colder, more viscous water and thus grains settle faster in warmer water. In essence, when a river warms by 25 °C owing to some combination of river elevation descent, flow to warmer latitudes, or seasonal increases, sediment transport will decrease: 90% for fine sand particles and 300% for fine silt grains[179]. This transport reduction with warming is in contrast to higher temperatures stimulating sediment production loaded into rivers. In Arctic settings, channel beds of small rivers remain frozen through the winter. Even when the spring freshet arrives, channel beds must first thaw before transport can begin and might delay bedload transport for several days in continuous permafrost terrain[180]. As for river temperatures, the global ocean has also progressively warmed since 1950, both at the surface and increasingly to depths exceeding 2,000 m (REF.[7]). The implications of a warming ocean for marine sediment transport remains an area for future research.

Precipitation changes in a warming world. If global runoff increases through the intensification of the hydrological cycle[181], then the carrying capacity of rivers should increase. In reality, hydrological processes are complex and intertwined with the dynamics of precipitation (snow, hail and droplet size) and evaporation (controlled by humidity, wind velocity and ground temperature), and spatially variable landcover dynamics (soil evaporation, canopy interception and transpiration). Discharge from the Mississippi River during the warm Mediaeval interval decreased, mostly owing to increases in evapotranspiration, implying that the lower Mississippi River's flows will decrease under a moderate warming scenario[182]. A more holistic understanding is needed of the impact of a warmer climate on the hydrological cycle and its impact on sediment loads.

The predicted intensification of the water cycle with warming will not be spatially homogeneous.

When applying a conservative climate scenario (RCP4.5, a representative concentration pathway trajectory adopted by the Intergovernmental Panel on Climate Change), river reaches in northeast India and East Asia are predicted to see increases in their flood intensity, an impact that might be smaller on other continents[183]. Over the past 30 years, annual discharge across the entire Arctic region has increased by around 10%, freshet discharge by 66%, and peak month discharge reduced by 7% (REF.[45]). Change in the melt month reflects a shift in snowmelt timing to favour longer ice-free periods[184]. From a sediment transport perspective, the largest impacts will arguably be from the redistribution of rainfall across the continental landscape. Changes in intra-basin precipitation dynamics are expected to increase or decrease the sediment loads of large tributaries, as high precipitation centres shift in locale. Regions with high relief and soft lithology will then amplify any increases in precipitation, by increasing their sediment yield in excess of increases in water discharge alone[185–187].

Desertification and wind intensities. Since 2010, global wind speeds over land have increased in response to internal decadal ocean and atmosphere oscillations[188]. This strengthening has increased potential wind energy by $17 \pm 2\%$ for 2010–2017 (REF.[188]). Aeolian-derived sediment transport is expected to increase with increases in terrestrial wind velocities and desertification[188], but has not been quantified. Climate variability and anthropogenic climate change, particularly through increases in both land surface air temperature and evapotranspiration, and decreases in precipitation in some dryland areas, are likely to have had a role, together with human action, in causing desertification[189]. Human drivers of desertification include expansion of croplands, unsustainable land management practices and land-use response to changes in population and regional economics. Vegetation loss and drying of surface cover due to desertification increases the frequency of dust storms and thus aeolian sediment transport[189].

Forest fires and sediment erosion. Most boreal forest fires begin from human recreation, but natural fires from lightning are responsible for larger burn areas, owing to slower detection speed and accessibility for fire fighters[190]. In Angola, savannah slash-and-burn practices are part of agricultural life, in contrast to the Congo and Brazil, where forest fires are largely tied to increases in net agricultural area. In the western USA, forest fires are more directly linked to climate trends and lightning clusters[191]. Between 1984 and 2011, the number of large fires in the USA increased by 7 per year, at a rate of 355 km² per year, most probably aided by climate change, flammable invasive species, and historical forest-management practices[192].

Forest fires increase the downslope transport of both fine and coarse suspended sediment, at rates about 35-fold greater than average, with sediment yields reaching 11,000 t km⁻² per year (REF.[192]) compared to the global average of 154 t km⁻² per year (REF.[16]). This sediment yield increase can reflect fire-induced changes to soils that become more hydrophobic[193], wherein post-fire

rainstorms increase rill development and induce mass movements. Where terrain is steep and incised and burn effects severe, debris flows can transport extremely large sediment masses[194,195]. Removal of vegetation is particularly relevant in fire-damaged arid regions[196,197]. Even physical weathering and sediment production from bedrock is markedly affected by wildfires; rock spalling is a common phenomenon after fires, although its effects on sediment yield remain unquantified[195]. If sediment evacuation accelerates in the aftermath of fires, sediment availability becomes the limiting factor in controlling post-fire sediment yields, particularly in zones receiving sufficient rainfall[198]. These effects are limited in spatial scale to the immediate burned area and to downstream channel corridors[198].

Acceleration of sea-level rise. During the past 4,200 years of the late Holocene, average sea level rise was 0.3 mm per year; since 1950, average sea level rise was 2.4 mm per year and is at present around 3.7 mm per year and increasing[7]. Variability within these eustatic trends relate to natural oscillations within the climate system: El Niño warming events, La Niña cold events, the Pacific Decadal Oscillation and the Atlantic Multidecadal Oscillation[199]. The impact of sea level rise on the global sediment budget includes the drowning of terrestrial land that directly translocates coastal sediment into the sea, and the increase in coastal energy with a near-shore deepening that increases the rate of coastal erosion. Regional rates of coastal erosion and drowning are being determined[47,94,126] but these satellite-based studies might miss real vulnerabilities if coastline protection infrastructure and coastal land-reclamation projects are not properly recognized[200] (TABLE 2).

Consequences of sediment flux changes

Sea level impacts of climate warming are compounded in sensitive coastal sedimentary environments, such as many river deltas where the sediment balance has been disrupted by reduced fluvial delivery owing to reservoir trapping, and as the land subsides through the local extraction of hydrocarbons and groundwater[39,201–203]. Delta subsidence beginning in the early twentieth century has become the dominant force affecting many coastal environments, overwhelming the global warming imprint on relative sea level[202]. The global scale of modern-day delta drowning is unprecedented in the past 7,000 years[204], as river loads diminish, sea levels rise, protective wetlands and mangroves are removed[85,202], and shoreline buffering is lost[202]. As a consequence, 48 deltas have an average relative sea level rise of 6.8 mm per year (REF.[205]), and 28 deltas have experienced severe flooding in the past decade. Coastal flooding is expected to increase by more than 50% under twenty-first-century projections[202]. Dams planned or under construction could add an additional 1 mm per year onto many deltas[205]. Increased river channelization and management will further reduce sediment retention on deltas, increasing relative sea level rise rates by another 2 mm or so per year (REF.[205]). Elevations on many deltas may also be lower than previously determined[206,207]. Consequently, some delta plains, such as the Po, Rhine, Tokyo lowland and Jakarta, are 3–4 m below sea level, protected by dykes. Land subsidence due to groundwater and gas pumping is now rigorously controlled in both Tokyo and central Bangkok[208].

Reduction in river discharge and loads has led to fewer functioning distributary channels; these abandoned delta channels and open delta flats are then tidally reworked. Since 1944 the Indus Delta has lost 12.7 km^2 per year (21% of the delta area) and coastal sediment has eroded at a net rate of about 47 Mt per year (REF.[126]). For subtropical deltas, marine sediment can be partly returned to a delta's surface through the action of storm surges[209,210]. Inhabited areas close to coastal fringes of the Ganges–Brahmaputra–Meghna Delta are protected by dykes of clay about 4–5 m, high reinforced with bricks[211]. However, storm surge heights can still be higher (>6.2 m during Cyclone Aila in 2009), causing embankment failures. Widespread flooding from Cyclone Aila deposited a thick (<1 m) layer of sand that devastated farms[211].

Many populated deltas are managed with active measures to protect critical infrastructure, including in the Mississippi, Rhine, and Yellow deltas. The Yellow River water-sediment regulation scheme, started in 2002, is an unprecedented engineering effort to mitigate siltation in both the lower river channel and within the upstream Xiaolangdi reservoir. Regulation methods increased the grain size of suspended sediment and decreased the suspended sediment concentration at the river mouth[212]. The pulsed delivery of muds and sands during dam releases returned the Yellow Delta to a short-lived accretion phase but riverbed erosion eventually decreased as the riverbed coarsened and the delta has reverted to a destructive phase since 2014 (REF.[101]).

Changes to the global sediment budget have also affected the maintenance of sandy beaches and a substantial proportion of the world's coastlines are already seeing erosion[213–216]. Thousands of kilometres of groins, jetties, seawalls, breakwaters and harbours have in turn led to either coastal erosion or siltation[47]. Mining of sand and gravel from coasts and rivers might have reached about 2 Gt per year (TABLE 2). Mining of beaches remains a problem for island states in the face of sea level rise (for example, Kiribati and the Marshall Islands)[217–219].

Limits to sediment flux estimations

Analysis of the global sediment budget highlights two intertwined limitations in securing the necessary comprehensive knowledge base to enable scientific progress in the field: a lack of global monitoring and reliance on modelling.

Most rivers have been monitored for their sediment load variability for too short a duration (a few years), with most observations made between 1960 and 1985 in the midst of prolific dam building[220]. The most effective way to determine the sediment load of a river is to sample across seasons, throughout high-intensity flood events[65,221] and, importantly, across a climate normal[222]. Only a few dozen rivers meet these sampling criteria; for the remaining >10,000 rivers and streams that discharge to the coastal ocean, either there are no measurements or observations are inadequate (see Supplementary Figure 1 for details). While some rivers meet the 30-year

monitoring requirement, the climate system has already shifted, such that vast differences can be seen between the 1981–2010 climate normal and the 1991–2020 normal: wet areas have become wetter and dry zones have become drier[223].

Advances in remote sensing may provide a way forward. For example, robust orbital microwave methods exist for measuring daily water discharge that are as accurate as gauging stations[224]. However, remote sensing of sediment concentrations in water relies on visible and near-infrared wavelengths that can be negatively impacted by tropospheric weather, such as cloud cover, and still requires some level of calibration to reduce error[24,225,226].

Models now play an important part in uncovering both historical and present-day flux values[179,185]. They have proved useful in combination with orbital sensors of the global environment[227]. Much work remains to improve models, particularly to capture historical and future trends of human impacts on the global environment[228]. The inability to accurately model human impacts on erosion and sediment transport in fluvial and coastal systems remains a bottleneck in the study of human–landscape interactions[16].

Summary and future perspectives

This Review reflects on the multi-faceted dimensions of a core Earth system process — the global sediment cycle — and the challenges of assembling a coherent picture of its past, present and future states (FIG. 5, Supplementary Table 4). The analysis presented here necessarily relies on a combination of empirical and

a Anthropocene land-to-sea sediment flux (Gt per year) in 2010
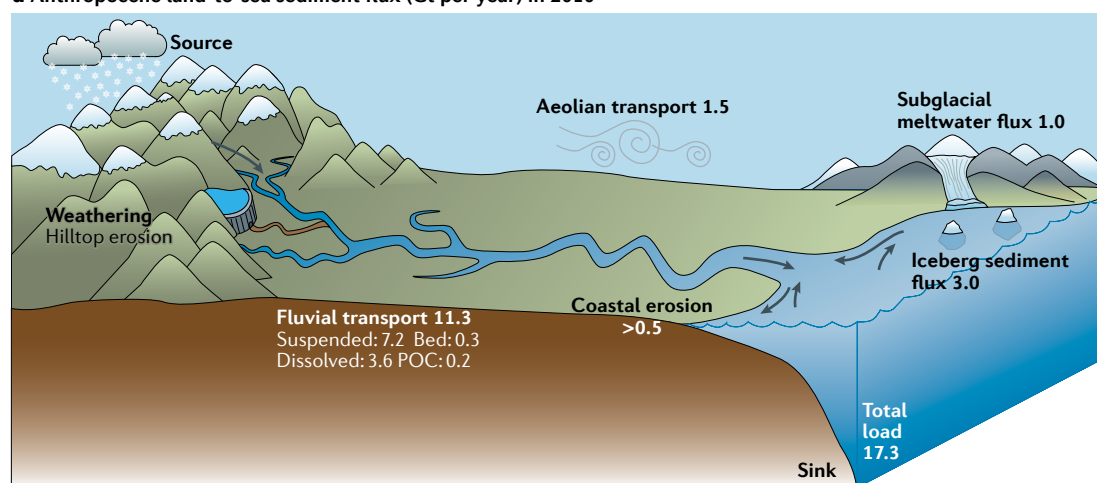
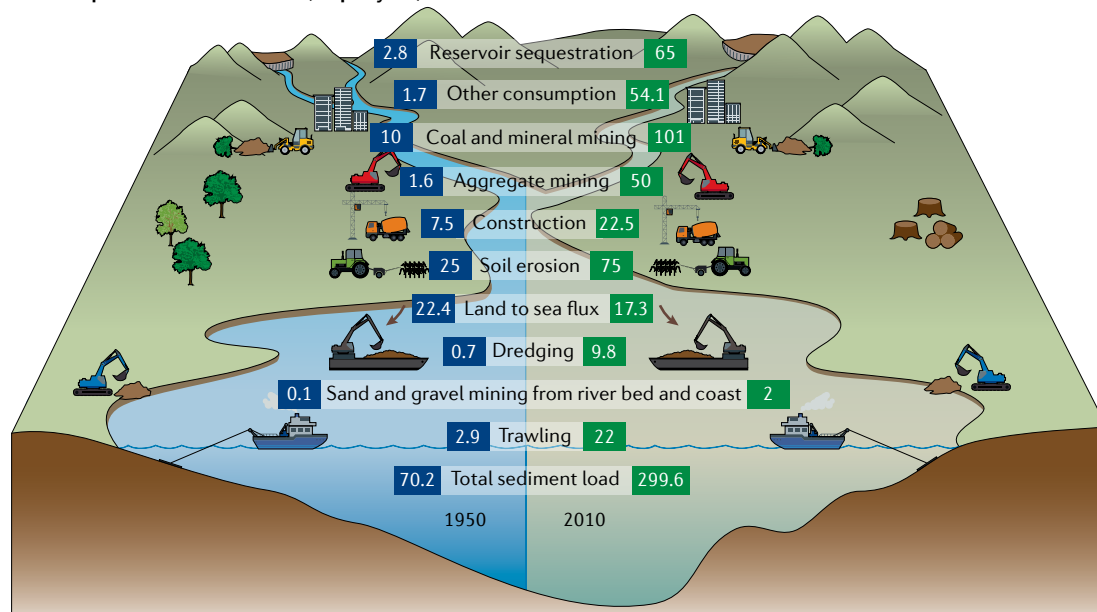**b Anthropocene sediment loads (Gt per year)**

Fig. 5 | **The increasing impact of human action on sediment fluxes and loads. a** | The land-to-sea directed terrestrial sediment fluxes off the landscape in Gt per year in 2010 (see TABLE 2 for the fluxes for 1950). **b** | A comparison of Anthropocene sediment loads for two representative years: 1950 and 2010. See TABLE 2 for further details and full references. Natural transport processes play an ever-decreasing part in the movement of sediment on Earth.

modelling studies, often fragmentary in space and time and representing various biogeophysical and socio-economic settings. The global sediment cycle is highly dynamic, playing out over diverse time- and spatial scales. Earth's sedimentary system was shaped over the geological past by natural forces but is today dominated by human actions controlling landscapes and hydrology and influencing climate change. The sediment cycle is not simply of academic interest but extends to the realm of societal vulnerabilities and risk management. The quest to protect human life and built infrastructure in the coastal zone pits massive engineering against major sedimentary forces that build and sustain deltas, with hundreds of millions of people at risk[203]. Developing a predictive sediment cycle model is essential to society's capacity to protect life and infrastructure.

Broad estimates of the substantial changes in Earth's sediment production and consumption and the diminishing role of natural processes that transport sediment are presented here (TABLE 2; FIG. 5). Employing only twenty-first-century climate warming scenarios, sediment delivery by rivers on average is expected to increase by 11–16% (REF.[229]), yet for deltas, mean and maximum declines are projected at 38% and 83%, respectively, between 1990–2019 and 2070–2099 (REF.[230]). While a contemporary global assessment highlights a key sustainable development issue, decision-makers will confront the legacy of historical changes and highly localized impacts of human actions. Scientists seeking to inform decision-making better must rapidly advance their capacity to make high-fidelity projections at these scales.

We propose that the research community join together in an 'Earth Sediment Cycle Grand Challenge' to develop a consensus-driven, comprehensive, authoritative, science-based geography of all aspects of the sediment cycle. The first phase could define contemporary conditions as the new baseline, followed by forecasts of future conditions and establishing a much improved mapping of the recent geological past. The content would include hotspots of sediment mobilization, transport and deposition; fluvial engineering; maps of the spatial and temporal distributions of sedimentary cycle changes; and societal assets potentially at risk, including populations, land uses and infrastructure assets. This challenge could establish an analytical framework incorporating datasets and process models depicting the individual elements in TABLE 2 and designed to accommodate new databases, knowledge and simulation capabilities as well as contributions from the social sciences, economics and history. Intercomparisons and data integration efforts, as with carbon modelling[231] and climate impacts[232], demonstrate the value of such collaborations in catalysing progress in the field. Model integration efforts with a strong sediment focus are ongoing and could offer leadership and strong international reach[233].

The proposed 'Earth Sediment Cycle Grand Challenge' opens the door to biogeophysical-engineering–social dimension analytics, which can be converted into best-practice guidelines for local planners and engineers, while still maintaining the global-scale context of the aggregate changes. This research-to-practice strategy would emphasize working with natural processes rather than against them and support society's need to manage an essential and ever-changing Earth system cycle, which increasingly could impose potentially serious, long-term, negative feedbacks on sustainable development.

1. Wilkinson, B. H. Humans as geologic agents: a deep-time perspective. *Geology* **33**, 161–164 (2005).
2. Syvitski, J. P. M., Vörösmarty, C., Kettner, A. J. & Green, P. Impact of humans on the flux of terrestrial sediment to the global coastal ocean. *Science* **308**, 376–380 (2005).
3. Meade, R. H. Movement and storage of sediment in river systems. In *Physical and Chemical Weathering in Geochemical Cycles* (eds Lerman, A. & Meybeck, M.) 165−179, (Springer, 1988).
4. Nicholas, A. P., Ashworth, P. J., Kirkby, M. J., Macklin, M. G. & Murray, T. Sediment slugs: large-scale fluctuations in fluvial sediment transport rates and storage volumes. *Prog. Phys. Geography Earth Environ.* **19**, 500−519 (1995).
5. Trimble, S. W. The fallacy of stream equilibrium in contemporary denudation studies. *Am. J. Sci.* **277**, 876–887 (1977).
6. Vörösmarty, C. J., Fekete, B. M., Meybeck, M. & Lammers, R. Global system of rivers: its role in organizing continental land mass and defining land-to-ocean linkages. *Glob. Biogeochem. Cycles* **14**, 599–621 (2000).
7. Syvitski, J. et al. Extraordinary human energy consumption and resultant geological impacts beginning around 1950 CE initiated the proposed Anthropocene Epoch. *Commun. Earth Environ.* **1**, 32 (2020).
8. Zalasiewicz, J. et al. When did the Anthropocene begin? A mid-twentieth century boundary level is stratigraphically optimal. *Quat. Int.* **383**, 196–203 (2015).
9. Waters, C. N. et al. The Anthropocene is functionally and stratigraphically distinct from the Holocene. *Science* **351**, aad2622 (2016).
10. Hay, W. H. Pleistocene–Holocene fluxes are not the Earth's norm. In *Global Sedimentary Geofluxes* (ed. Hay, W. H.) 15−27 (National Academy of Sciences Press, 1994).
11. Walling, D. E. & Webb, B. W. Erosion and sediment yield: a global overview. In *Erosion and Sediment Yield: Global and Regional Perspectives* 3−19 (IAHS, 1996).
12. Syvitski, J. P. M. Sediment fluxes and rates of sedimentation. In *Encyclopedia of Sediments and Sedimentary Rocks* (ed. Middleton, G. V.) 600−606 (Kluwer Academic, Netherlands, 2003).
13. Hallet, B., Hunter, L. & Bogen, J. Rates of erosion and sediment evacuation by glaciers: a review of field data and their implications. *Glob. Planet. Change* **12**, 213−235 (1996).
14. Métivier, F., Gaudemer, Y., Tapponnier, P. & Klein, M. Mass accumulation rates in Asia during the Cenozoic. *Geophys. J. Int.* **137**, 280−318 (1999).
15. Latrubesse, E. M. & Restrepo, J. D. Sediment yield along the Andes: continental budget, regional variations, and comparisons with other basins from orogenic mountain belts. *Geomorphology* **216**, 225−233 (2014).
16. Syvitski, J. P. M. & Milliman, J. D. Geology, geography, and humans battle for dominance over the delivery of sediment to the coastal ocean. *J. Geol.* **115**, 1−19 (2007).
17. Syvitski, J. P. M. & Kettner, A. J. Sediment flux and the Anthropocene. *Phil. Trans. R. Soc. A* **369**, 957−975 (2011).
18. Milliman, J. D. & Syvitski, J. P. M. Geomorphic/tectonic control of sediment discharge to the ocean: the importance of small mountainous rivers. *J. Geol.* **100**, 525−544 (1992).
19. Holmes, R. M. et al. A circumpolar perspective on fluvial sediment flux to the Arctic ocean. *Glob. Biogeochem. Cycles* **16**, 45-1−45-14 (2002).
20. Gordeev, V. V. Fluvial sediment flux to the Arctic Ocean. *Geomorphology* **80**, 94−104 (2006).
21. Syvitski, J. P., Kettner, A. J., Overeem, I., Brakenridge, G. R. & Cohen, S. Latitudinal controls on siliciclastic sediment production and transport. In *Latitudinal Controls on Stratigraphic Models and Sedimentary Concepts* 14−28 (eds Fraticelli, C. M., Martinius, A. W., Markwick, P. & Suter, J. R.) (Geological Society Special Publication, 2019).
22. Dadson, S. J. et al. Earthquake triggered increase in sediment delivery from an active mountain belt. *Geology* **32**, 733−736 (2004).
23. Hovius, N. et al. Prolonged seismically induced erosion and the mass balance of a large earthquake. *Earth Planet. Sci. Lett.* **3−4**, 347−355 (2011).
24. Overeem, I. et al. Substantial export of suspended sediment to the global oceans from glacial erosion in Greenland. *Nat. Geosci.* **10**, 859−863 (2017).
25. Steinberger, B. Topography caused by mantle density variations: observation-based estimates and models derived from tomography and lithosphere thickness. *Geophys. J. Int.* **205**, 604−621 (2016).
26. Stallard, R. Terrestrial sedimentation and the carbon cycle: coupling weathering and erosion to carbon burial. *Glob. Biogeochem. Cycles* **12**, 231−257 (1998).
27. Syvitski, J. P. M., Overeem, I., Brakenridge, G. R. & Hannon, M. D. Floods, floodplains, delta plains — a satellite imaging approach. *Sediment. Geol.* **267/268**, 1−14 (2012).
28. Kettner, A. J., Restrepo, J. D. & Syvitski, J. P. M. A spatial simulation experiment to replicate the fluvial sediment fluxes within the Magdalena River Basin, Colombia. *J. Geol.* **118**, 363−379 (2010).
29. Chen, Z., Wang, Z., Finlayson, B., Chen, J. & Yin, D. Implications of flow control by the Three Gorges Dam on sediment and channel dynamics of the middle Yangtze (Changjiang) River, China. *Geology* **38**, 1043−1046 (2010).

REVIEWS

30. Wilkinson, B. H. & McElroy, B. J. The impact of humans on continental erosion and sedimentation. *Geol. Soc. Am. Bull.* **119**, 140–156 (2007).

31. Beach, T. The fate of eroded soil: sediment sinks and sediment budgets of agrarian landscapes in southern Minnesota, 1851–1988. *Ann. Assoc. Am. Geogr.* **84**, 5–28 (1994).

32. Restrepo, J. D., Kettner, A. J. & Syvitski, J. P. Recent deforestation causes rapid increase in river sediment load in the Colombian Andes. *Anthropocene* **10**, 13–28 (2015).

33. Smith, S. V., Renwick, W. H., Buddemeier, R. W. & Crossland, C. J. Budgets of soil erosion and deposition for sediments and sedimentary organic carbon across the conterminous United States. *Glob. Biogeochem. Cycles* **15**, 697 (2001).

34. Ibáñez, C. et al. Basin-scale land use impacts on world deltas: human vs natural forcings. *Glob. Planet. Change* **173**, 24–32 (2019).

35. Curtis, W. F., Culbertson, K. & Chase, E. B. Fluvial-sediment discharge to the oceans from the conterminous United States. *US Geol. Surv. Circ.* **670**, 1–17 (1973).

36. Chen, Z., Syvitski, J. P. M., Gao, S., Overeem, I. & Kettner, A. J. Socio-economic impacts on flooding: a 4000-year history of the Yellow River, China. *Ambio* **41**, 682–698 (2012).

37. Zhou, L. Y. et al. Coastal erosion as a major sediment supplier to continental shelves: example from the abandoned Old Huanghe (Yellow River) delta. *Continental Shelf Res.* **82**, 43–59 (2014).

38. Zhou, L. et al. Sediment budget of the Yellow River delta during 1959–2012, estimated from morphological changes and accumulation rates. *Mar. Geol.* **430**, 106363 (2020).

39. Ericson, J. P., Vörösmarty, C. J., Dingman, S. L., Ward, L. G. & Meybeck, M. Effective sea-level rise in deltas: sources of change and human-dimension implications. *Glob. Planet. Change* **50**, 63–82 (2006).

40. Walsh, J. P. & Nittrouer, C. A. Understanding fine-grained river-sediment dispersal on continental margins. *Mar. Geol.* **263**, 34–45 (2009).

41. Bernhardt, A. & Schwanghart, W. Where and why do submarine canyons remain connected to the shore during sealevel rise? — Insights from global topographic analysis and Bayesian regression. *Geophys. Res. Lett.* **48**, e2020GL092234 (2021).

42. Morehead, M. D., Syvitski, J. P. M., Hutton, E. W. H. & Peckham, S. D. Modelling the temporal variability in the flux of sediment in ungauged river basins. *Glob. Planet. Change* **39**, 95–110 (2003).

43. Meybeck, M., Laroche, L., Darr, H. H. & Syvitski, J. P. M. Global variability of daily total suspended solids and their fluxes in rivers. *Glob. Planet. Change* **39**, 65–93 (2003).

44. Paszkowski, A., Goodbred, S., Borgomeo, E., Shah Alam Khan, M. & Hall, J. W. Geomorphic change in the Ganges–Brahmaputra–Meghna delta. *Nat. Rev. Earth Environ.* **2**, 763–780 https://www.nature.com/articles/s43017-021-00213-4 (2021).

45. Overeem, I. & Syvitski, J. P. M. Shifting discharge peaks in Arctic rivers 1977–2007. *Geogr. Ann. A* **92**, 285–296 (2010).

46. Rawlins, M. A. et al. Analysis of the Arctic system for freshwater cycle intensification: observations and expectations. *J. Clim.* **23**, 5715–5737 (2010).

47. Syvitski, J. P. M. et al. Dynamics of the coastal zone. In *Coastal Fluxes in the Anthropocene* 39–94 (eds Crossland, C. J., Kremer, H. H., Lindeboom, H. J., Marshall Crossland, J. I. & Le Tissier, M. D. A.) (Springer, 2005).

48. Syvitski, J. P. M., Morehead, M. D., Bahr, D. & Mulder, T. Estimating fluvial sediment transport: the rating parameters. *Wat. Resour. Res.* **36**, 2747–2760 (2000).

49. N'kaya, G. D. M., Orange, D., Bayonne Padou, S. M., Datok, P. & Laraque, A. Temporal variability of sediments, dissolved solids and dissolved organic matter fluxes in the Congo river at Brazzaville/Kinshasa. *Geosciences* **10**, 341 (2020).

50. Huang, T.-H., Fu, Y.-H., Pan, P-Y. & Chen, C.-T. A. Fluvial carbon fluxes in tropical rivers. *Curr. Opin. Environ. Sustain.* **4**, 162–169 (2012).

51. Lyons, W. B., Nezat, C. A., Carey, A. E. & Hicks, D. M. Organic carbon fluxes to the ocean from high-standing islands. *Geology* **30**, 443–446 (2002).

52. Beusen, A. H. W., Dekkers, A. L. M., Bouwman, A. F., Ludwig, W. & Harrison, J. Estimation of global river transport of sediments and associated particulate C, N, and P. *Glob. Biogeochem. Cycles* **19**, GB4S05 (2005).

53. Bianchi, T. S. et al. Centers of organic carbon burial and oxidation at the land–ocean interface. *Org. Geochem.* **115**, 138–155 (2018).

54. Burdige, D. J. Burial of terrestrial organic matter in marine sediments: a reassessment. *Glob. Biogeochem. Cycles* **19**, GB4011 (2005).

55. Qiao, J. et al. Runoff-driven export of terrigenous particulate organic matter from a small mountainous river: sources, fluxes and comparisons among different rivers. *Biogeochemistry* **147**, 71–86 (2020).

56. Usman, M. O. et al. Reconciling drainage and receiving basin signatures of the Godavari River system. *Biogeosciences* **15**, 3357–3375 (2018).

57. Pradhan, U. K. et al. Multi-proxy evidence for compositional change of organic matter in the largest tropical (peninsula) river basin of India. *J. Hydrol.* **519**, 999–1009 (2014).

58. Gruca-Rokosz, R. Quantitative fluxes of the greenhouse gases CH_4 and CO_2 from the surfaces of selected Polish reservoirs. *Atmosphere* **11**, 286 (2020).

59. Zalasiewicz, J. et al. The geological cycle of plastics and their use as a stratigraphic indicator of the Anthropocene. *Anthropocene* **13**, 4–17 (2016).

60. Geyer, R., Jambeck, J. R. & Law, K. L. Production, use, and fate of all plastics ever made. *Sci. Adv.* **3**, e1700782 (2017).

61. Jambeck, J. R. et al. Plastic waste inputs from land into the ocean. *Science* **347**, 768–771 (2015).

62. Bergmann, M. et al. White and wonderful? Microplastics prevail in snow from the Alps to the Arctic. *Sci. Adv.* **5**, eaax1157 (2019).

63. Probst, J. L. & Tardy, Y. Global runoff fluctuations during the last 80 years in relation to world temperature change. *Am. J. Sci.* **289**, 267–285 (1989).

64. Knox, J. C. Large increase in flood magnitude in response to modest changes in climate. *Nature* **361**, 430–432 (1993).

65. Milliman, J. D. & Kao, S. J. Hyperpycnal discharge of fluvial sediment to the ocean: impact of super-typhoon Herb (1996) on Taiwanese rivers. *J. Geol.* **113**, 503–516 (2005).

66. Wang, H. et al. Recent changes of sediment flux to the western Pacific Ocean from major rivers in east and southeast Asia. *Earth Sci. Rev.* **108**, 80–100 (2011).

67. Depetris, P. J., Kempe, S., Latif, M. & Mook, W. G. ENSO controlled flooding in the Parana River (1904-1991). *Naturwissenschaften* **83**, 127–129 (1996).

68. Vörösmarty, C. J. et al. Analyzing the discharge regime of a large tropical river through remote sensing, ground-based climatic data, and modelling. *Water Resour. Res.* **32**, 3137–3150 (1996).

69. Restrepo, J. D. & Kjerfve, B. Magdalena river: interannual variability (1975–1995) and revised water discharge and sediment load estimates. *J. Hydrol.* **235**, 137–149 (2000).

70. Mulder, T. & Syvitski, J. P. M. Climatic and morphologic relationships of rivers. Implications of sea level fluctuations on river loads. *J. Geol.* **104**, 509–523 (1996).

71. Poag, C. W. U.S. middle Atlantic continental rise: provenance, dispersal, and deposition of Jurassic to Quaternary sediments. In *Geologic Evolution of Atlantic Continental Rises* 100–156 (eds Poag, C. W. & Graciansky, P. C.) (Van Nostrand Reinhold, 1992).

72. Elverhøi, A., Hooke, R. L. & Solheim, A. Late Cenozoic erosion and sediment yield from the Svalbard-Barents Sea region; implications for understanding erosion of glacierized basins. *Quat. Sci. Rev.* **17**, 209–241 (1998).

73. O'Grady, D. B. & Syvitski, J. P. M. Large-scale morphology of Arctic continental slopes: the influence of sediment delivery on slope form. In *Glacier-Influenced Sedimentation on High-Latitude Continental Margins* (eds Dowdeswell, J. A. & O'Cofaigh, C.) 11–31 (Geological Society, 2002).

74. Goodbred, S. L. & Kuehl, S. A. Holocene and modern sediment budgets for the Ganges–Brahmaputra river system: evidence for highstand dispersal to floodplain, shelf and deep-sea depocenters. *Geology* **27**, 559–562 (1999).

75. Kettner, A. J. & Syvitski, J. P. M. Predicting discharge and sediment flux of the Po River, Italy since the Late Glacial Maximum. In *Analogue and Numerical Forward Modelling of Sedimentary Systems: from Understanding to Prediction* (eds De Boer, P. L., Postma, G., van der Zwan, C. J., Burgess, P. M. & Kukla, P.) 171–189 (International Association of Sedimentologists, 2008).

76. Goodbred, S. L. & Kuehl, S. A. Enormous Ganges–Brahmaputra sediment discharge during strengthened early Holocene monsoon. *Geology* **28**, 1083–1086 (2000).

77. Wang, Z. et al. Three-dimensional evolution of the Yangtze River mouth, China during the Holocene: impacts of sea level, climate and human activity. *Earth Sci. Rev.* **185**, 938–955 (2018).

78. Jenny, J. P. et al. Human and climate global-scale imprint on sediment transfer during the Holocene. *Proc. Natl Acad. Sci. USA* **116**, 22972–22976 (2019).

79. Sima, R. J. A dirty truth: humans began accelerating soil erosion 4,000 years ago. *Eos* https://doi.org/10.1029/2019EO137634 (2019).

80. Wu, Z. et al. Anthropogenic impacts on the decreasing sediment loads of nine major rivers in China, 1954–2015. *Sci. Total. Environ.* **739**, 139653 (2020).

81. Wu, X. et al. Climate and humans battle for dominance over the Yellow River's sediment discharge: from the Mid-Holocene to the Anthropocene. *Mar. Geol.* **425**, 106188 (2020).

82. Kong, R. et al. Increasing carbon storage in subtropical forests over the Yangtze River basin and its relations to the major ecological projects. *Sci. Total. Environ.* **709**, 136163 (2020).

83. Kettner, A. J., Gomez, B. & Syvitski, J. P. M. Modeling suspended sediment discharge from the Waipaoa River system, New Zealand: the last 3000 years. *Water Resour. Res.* **43**, W07411 (2007).

84. Giosan et al. Massive erosion in monsoonal central India linked to late Holocene land cover degradation. *Earth Surf. Dynam.* **5**, 781–789 (2017).

85. Meybeck, M. & Vörösmarty, C. J. Fluvial filtering of land to ocean fluxes: from natural Holocene variations to Anthropocene. *Comptes Rendus* **337**, 107–123 (2005).

86. Tréguer, P. J. & De La Rocha, C. L. The world ocean silica cycle. *Annu. Rev. Mar. Sci.* **5**, 477–501 (2013).

87. Isson, T. T. & Planavsky, N. J. Reverse weathering as a long-term stabilizer of marine pH and planetary climate. *Nature* **560**, 471–475 (2018).

88. Tréguer, P. et al. Reviews and syntheses: the biogeochemical cycle of silicon in the modern ocean. *Biogeosciences* **18**, 1269–1289 (2021).

89. Leithold, E. L. & Blair, N. E. Watershed control on the carbon loading of marine sedimentary particles. *Geochim. Cosmochim. Acta* **65**, 2231–2240 (2001).

90. Nittrouer, C. A. et al. Writing a Rosetta stone: insights into continental-margin sedimentary processes and strata. In *Continental-Margin Sedimentation: From Sediment Transport to Sequence Stratigraphy* (eds Nittrouer, C. A. et al.) 1–48 (IAS, 2007).

91. Milliman, J. D. & Farnsworth, K. L. *River Discharge to the Coastal Ocean* 384 (Cambridge Univ. Press, 2011).

92. Tanaka, T. Y. & Chiba, M. A numerical study of the contributions of dust source regions to the global dust budget. *Glob. Planet. Change* **52**, 88–104 (2006).

93. Maher, B. A. et al. Global connections between aeolian dust, climate and ocean biogeochemistry at the present day and at the Last Glacial Maximum. *Earth Sci. Rev.* **99**, 61–97 (2010).

94. Saito, Y., Chaimanee, N., Jarupongsakul, T. & Syvitski, J. P. M. Shrinking megadeltas in Asia: sea-level rise and sediment reduction impacts from case study of the Chao Phraya delta. *Inprint Newsletter of the IGBP/IHDP Land Ocean Interaction in the Coastal Zone* **2007/2**, 3–9 (2007).

95. Latrubesse, E. M., Amsler, M. L., de Morais, R. P. & Aquino, S. The geomorphologic response of a large pristine alluvial river to tremendous deforestation in the South American tropics: the case of the Araguaia River. *Geomorphology* **113**, 239–252 (2009).

96. Restrepo, J. D. & Syvitski, J. P. M. Assessing the effect of natural controls and land use change on sediment yield in a major Andean river: the Magdalena drainage basin, Colombia. *Ambio* **35**, 65–74 (2006).

97. Wang, H., Yang, Z., Saito, Y., Liu, J. P. & Sun, X. Stepwise decreases of the Huanghe (Yellow River) sediment load (1950–2004): impacts from climate changes and human activities. *Glob. Planet. Change* **57**, 331–354 (2007).

98. Chen, Y., Overeem, I., Gao, S., Syvitski, J. P. M. & Kettner, A. J. Quantifying sediment storage on the floodplains outside levees along the lower Yellow River during the years 1580–1849. *Earth Surf. Process. Landf.* **44**, 581–594 (2018).

99. Syvitski, J. P. M., Kettner, A., Peckham, S. D. & Kao, S. J. Predicting the flux of sediment to the coastal zone: application to the Lanyang watershed, northern Taiwan. *J. Coast. Res.* **21**, 580–587 (2005).

100. Walling, D. E. & Fang, D. Recent trends in the suspended sediment loads of the world's rivers. *Glob. Planet. Change* **39**, 111–126 (2003).

101. Wu, X. et al. Can reservoir regulation along the Yellow River be a sustainable way to save a sinking delta? *Earths Future* **8**, e2020EF001587 (2020).
102. Syvitski, J. P. M. Deltas at risk. *Sustain. Sci.* **3**, 23–32 (2008).
103. Kondolf, G. M. et al. Changing sediment budget of the Mekong: cumulative threats and management strategies for a large river basin. *Sci. Total. Environ.* **625**, 114–134 (2018).
104. Syvitski, J. P. M. & Brakenridge, G. R. Causation and avoidance of catastrophic flooding along the Indus River, Pakistan. *GSA Today* **23**, 4–10 (2013).
105. Cooper, A. H., Brown, T. J., Price, S. J., Ford, J. R. & Waters, C. N. Humans are the most significant global geomorphological driving force of the 21st century. *Anthropocene Rev.* **5**, 222–229 (2018).
106. Global Aggregates Information Network (GAIN). GAIN newsletter #4, January 2019. *GAIN* https://www.gain.ie/s/GAIN_Newsletter_Jan19.pdf (2019).
107. Waters, C. N. & Zalasiewicz, J. Concrete: the most abundant novel rock type of the Anthropocene. In *The Encyclopedia of the Anthropocene* Vol. 1 75–85 (eds Sala, D. A. D. & Goldstein, M. I.) (Elsevier, 2018).
108. Kemp, D. B., Sadler, P. M. & Vanacker, V. The human impact on North American erosion, sediment transfer, and storage in a geologic context. *Nat. Commun.* **11**, 6012 (2020).
109. Montgomery, D. R. Soil erosion and agricultural sustainability. *Proc. Natl Acad. Sci. USA* **104**, 133268–133272 (2007).
110. Reusser, L., Bierman, P. & Rood, D. Quantifying human impacts on rates of erosion and sediment transport at a landscape scale. *Geology* **43**, 171–174 (2014).
111. Bonachea, J. et al. Natural and human forcing in recent geomorphic change; case studies in the Rio de la Plata basin. *Sci. Total. Env.* **408**, 2674–2695 (2010).
112. Liu et al. Global vegetation biomass change (1988–2008) and attribution to environmental and human drivers. *Glob. Ecol. Biogeogr.* **22**, 692–705 (2013).
113. Faour, G. et al. Global trends analysis of the main vegetation types throughout the past four decades. *Appl. Geogr.* **97**, 184–195 (2018).
114. Hooke, R. L. On the history of humans as geomorphic agents. *Geology* **28**, 843–846 (2000).
115. Borrelli, P. et al. An assessment of the global impact of 21st century land use change on soil erosion. *Nat. Commun.* **8**, 2013 (2017).
116. Harden, D. R. A comparison of flood-producing storms and their impacts in northwestern California. In *Geomorphic Processes and Aquatic Habitat in the Redwood Creek Basin, Northwestern California*. US Geological Survey Professional Paper 1454, D1–D9 (USGS, 1995).
117. Hewawasam, T., von Blanckenburg, F., Schaller, M. & Kubik, P. Increase of human over natural erosion rates in tropical highlands constrained by cosmogenic nuclides. *Geology* **31**, 597–600 (2003).
118. Vörösmarty, C. et al. Anthropogenic sediment retention: major global-scale impact from the population of registered impoundments. *Glob. Planet. Change* **39**, 169–190 (2003).
119. Best, J. Anthropogenic stresses on the world's big rivers. *Nat. Geosci.* **12**, 7–21 (2019).
120. Grill, G. et al. Mapping the world's free-flowing rivers. *Nature* **569**, 215–221 (2019).
121. Zarfl, C., Lumsdon, A. E., Berlekamp, J., Tydecks, L. & Tockner, K. Global boom in hydropower dam construction. *Aquat. Sci.* **77**, 161–170 (2015).
122. International Commission on Large Dams. World Register of Dams: general synthesis. *WRD* http://www.icold-cigb.org/GB/world_register/general_synthesis.asp (2017).
123. Syvitski, J. P., Zalasiewicz, J. & Summerhayes, C. Changes to Holocene/Anthropocene patterns of sedimentation from terrestrial to marine. In *The Anthropocene as a Geological Time Unit: A Guide to the Scientific Evidence and Current Debate* (eds Zalasiewicz, J., Waters, C., Williams, M. & Summerhayes, C.) 90–108 (Cambridge Univ. Press, 2019).
124. Syvitski, J. P. M., Kettner, A. J., Correggiari, A. & Nelson, B. W. Distributary channels and their impact on sediment dispersal. *Mar. Geol.* **222/223**, 75–94 (2005).
125. Syvitski, J. P. M. & Kettner, A. J. On the flux of water and sediment into the Northern Adriatic. *Continental Shelf Res.* **27**, 296–308 (2007).
126. Syvitski, J. P. M. et al. Anthropocene metamorphosis of the Indus delta and lower floodplain. *Anthropocene* **3**, 24–35 (2013).
127. Laruelle, G. G. et al. Anthopogenic perturbations of the silicon cycle at the global scale: key role of the land-ocean transition. *Glob. Biogeochem. Cycles* **23**, GB4031 (2009).
128. Harmer, O. P. & Clifford, N. J. Geomorphological explanation of the long profile of the Lower Mississippi River. *Geomorphology* **84**, 222–240 (2007).
129. Galat, D. L. A. O. Flooding to restore connectivity of regulated, large-river wetlands: natural and controlled flooding as complementary processes along the lower Missouri River. *Bioscience* **48**, 721–733 (1998).
130. Day, J. W., Lane, R. R., D'Elia, C. & Kemp, G. P. Large infrequently operated river diversions for Mississippi delta restoration. *Estuar. Coast. Shelf Sci.* **183**, 1–12 (2016).
131. Higgins, S. A., Overeem, I., Rogers, K. G. & Kalina, E. A. River linking in India: downstream impacts on water discharge and suspended sediment transport on deltas. *Elem. Sci. Anthrop.* **6**, 20 (2018).
132. Monteiro, P. J. M. et al. Towards sustainable concrete. *Nat. Mater.* **16**, 698–699 (2017).
133. Filho, W. L. et al. The unsustainable use of sand: reporting on a global problem. *Sustainability* **13**, 3356 (2021).
134. Kamboj, V., Kamboj, N. & Sharma, S. Environmental impact of riverbed mining — a review. *Intl. J. Sci. Res. Rev.* **7**, 504–520 (2017).
135. Mechi, A. & Sanches, D. L. The environmental impact of mining in the state of São Paulo. *Estudos Avançados* **24**, 209–220 (2010).
136. Bisht, A. & Gerber, J. F. Ecological distribution conflicts (EDCs) over mineral extractivism in India: an overview. *Extract. Indust. Soc.* **4**, 548–563 (2017).
137. Bisht, A. Discontent, conflict, social resistance and violence at non-metallic mining frontiers in India. *Ecol. Econ. Soc.* **2**, 31–42 (2019).
138. Bisht, A. Conceptualizing sand extractivism: deconstructing an emerging resource frontier. *Extract. Indust. Soc.* **8**, 100904 (2021).
139. Bravard, J.-P. et al. Geography of sand and gravel mining in the Lower Mekong River. *EchoGeo* http://echogeo.revues.org/13659 (2013).
140. Hackney, C. R. et al. Sand mining far outpaces natural supply in a large alluvial river. *Earth Surf. Dyn.* **9**, 1323–1334 (2021).
141. Hackney, C. R. et al. Riverbank instability from unsustainable sand mining in the lower Mekong River. *Nat. Sustain.* **3**, 217–225 (2020).
142. United Nations. Import of natural sand except sand for mineral extraction as reported. *United Nations Commodity Trade Statistics Database* http://comtrade.un.org (2014).
143. Torres, A., Brandt, J., Lear, K. & Liu, J. A looming tragedy of the sand commons. *Science* **357**, 970–971 (2017).
144. James, J. et al. The effective development of offshore aggregates in south-east Asia. Technical Report WC/99/9 (British Geological Survey, 1999).
145. Jia, L. et al. Impacts of the large amount of sand mining on riverbed morphology and tidal dynamics in lower reaches and delta of the Dongjiang River. *J. Geogr. Sci.* **17**, 197–211 (2007).
146. Velegrakis, A. F. et al. European marine aggregates resources: origins, usage, prospecting and dredging techniques. *J. Coast. Res.* **51**, 1–14 (2010).
147. Amoroso, R. O. et al. Bottom trawl fishing footprints on the world's continental shelves. *Proc. Natl Acad. Sci. USA* **115**, E10275–E10282 (2018).
148. Martín, J., Puig, P., Masqué, P., Palanques, A. & Sánchez-Gómez, A. Impact of bottom trawling on deep-sea sediment properties along the flanks of a submarine canyon. *PLoS ONE* **9**, e104536 (2014).
149. Paradis, S. et al. Bottom trawling along submarine canyons impacts deep sedimentary regimes. *Sci. Rep.* **7**, 43332 (2017).
150. Oberle, F. K. J., Storlazzi, C. D. & Hanebuth, T. J. J. What a drag: quantifying the global impact of chronic bottom trawling on continental shelf sediment. *J. Mar. Syst.* **159**, 109–119 (2016).
151. GISTEMP Team. GISS surface temperature analysis (GISTEMP), version 4. *NASA Goddard Institute for Space Studies* http://data.giss.nasa.gov/gistemp/ (2021).
152. Lenssen, N. J. L. et al. Improvements in the GISTEMP uncertainty model. *J. Geophys. Res. Atmos.* **124**, 6307–6326 (2019).
153. Schmidt, G. A., Ruedy, R. A., Miller, R. L. & Lacis, A. A. Attribution of the present-day total greenhouse effect. *J. Geophys. Res.* **115**, D20106 (2010).
154. Zanna, L., Khatiwala, S., Gregory, J. M., Ison, J. & Helmbach, P. Global reconstruction of historical ocean heat storage and transport. *Proc. Natl Acad. Sci. USA* **116**, 1126–1131 (2019).
155. Rempel, A. W., Marshall, J. A. & Roering, J. J. Modeling relative frost weathering rates at geomorphic scales. *Earth Planet. Sci. Lett.* **453**, 87–95 (2016).
156. Syvitski, J. P. M., Peckham, S. D., Hilberman, R. D. & Mulder, T. Predicting the terrestrial flux of sediment to the global ocean: a planetary perspective. *Sediment. Geol.* **162**, 5–24 (2003).
157. Farquharson, L. M. et al. Climate change drives widespread and rapid thermokarst development in very cold permafrost in the Canadian high Arctic. *Geophys. Res. Lett.* **46**, 6681–6689 (2019).
158. Kokelj, S. V. et al. Thawing of massive ground ice in mega slumps drives increases in stream sediment and solute flux across a range of watershed scales. *J. Geophys. Res. Earth Surf.* **118**, 681–692 (2013).
159. Syvitski, J. P. M. Sediment discharge variability in Arctic rivers: implications for a warmer future. *Polar Res.* **21**, 323–330 (2002).
160. Li, D. et al. Exceptional increases in fluvial sediment fluxes in a warmer and wetter high mountain Asia. *Science* **374**, 599–603 (2021).
161. Syvitski, J. P. M. & Andrews, J. T. Climate change: numerical modelling of sedimentation and coastal processes, Eastern Canadian Arctic. *Arctic Alpine Res.* **26**, 199–212 (1994).
162. Van der Broeke, M. et al. On the recent contribution of the Greenland ice sheet to sea level change. *Cryosphere* **10**, 1933–1946 (2016).
163. Bendixen, M. et al. Delta progradation in Greenland driven by increasing glacial mass loss. *Nature* **550**, 101–104 (2017).
164. Bamber, J. L., Westaway, R. M., Marzeion, B. & Wouters, B. The land ice contribution to sea level during the satellite era. *Environ. Res. Lett.* **13**, 063008 (2018).
165. Mankoff, K. D. et al. Greenland Ice Sheet solid ice discharge from 1986 through March 2020. *Earth Syst. Sci. Data* **12**, 1367–1383 (2020).
166. Hugelius, G. et al. Estimated stocks of circumpolar permafrost carbon with quantified uncertainty ranges and identified data gaps. *Biogeosciences* **11**, 6573–6593 (2014).
167. Zimov, S. A. et al. Permafrost carbon: stock and decomposability of a globally significant carbon pool. *Geophys. Res. Lett.* **33**, L20502 (2006).
168. Turetsky, M. R. et al. Carbon release through abrupt permafrost thaw. *Nat. Geosci.* **13**, 138–143 (2020).
169. Schaefer, K., Lantuit, H., Romanovsky, V. E., Schuur, E. A. G. & Witt, R. The impact of the permafrost carbon feedback on global climate. *Environ. Res. Lett.* **9**, 085003 (2014).
170. Olefeldt, D. et al. Circumpolar distribution and carbon storage of thermokarst landscapes. *Nat. Commun.* **7**, 13043 (2016).
171. Schweiger, A., Zhang, J., Lindsay, R., Steele, M. & Stern, H. PIOMAS arctic sea ice volume reanalysis. *Polar Science Centre* http://psc.apl.uw.edu/research/projects/arctic-sea-ice-volume-anomaly/ (2019).
172. Overeem, I. et al. Sea ice loss enhances wave action at the Arctic coast. *Geophys. Res. Lett.* **38**, L17503 (2011).
173. Crawford, A. D. & Serreze, M. C. Projected changes in the Arctic frontal zone and summer Arctic cyclone activity in the CESM large ensemble. *J. Clim.* **30**, 9847–9869 (2017).
174. Jones, B. M. et al. Increase in the rate and uniformity of coastline erosion in Arctic Alaska. *Geophys. Res. Lett.* **36**, L03503 (2009).
175. Gibbs, A. E., Ohman, K. A., Coppersmith, R. & Richmond, B. M. *National Assessment of Shoreline Change: A GIS Compilation of Updated Vector Shorelines and Associated Shoreline Change Data for the North Coast of Alaska, U.S. Canadian border to Icy Cape* (US Geological Survey, 2017).
176. Lantuit, H. et al. The Arctic coastal dynamics database: a new classification scheme and statistics on arctic permafrost coastlines. *Estuaries Coasts* **35**, 383–400 (2012).
177. Barnhart, K. R. et al. Modelling erosion of ice-rich permafrost bluffs along the Alaskan Beaufort Sea coast. *J. Geophys. Res. Earth* **119**, 1155–1179 (2014).
178. Barnhart, K. R., Overeem, I. & Anderson, R. S. The effect of changing sea ice on the physical vulnerability of Arctic coasts. *Cryosphere* **8**, 1777–1799 (2014).
179. Syvitski, J., Cohen, S., Miara, A. & Best, J. River temperature and the thermal-dynamic transport of sediment. *Glob. Planet. Change* **178**, 168–183 (2019).

REVIEWS

180. Scott, K. M. *Effects of Permafrost on Stream Channel Behavior in Arctic Alaska* USGS Professional Paper 1068, 1–19 (US Geological Survey, 1978).

181. Madakumbura, G. D. et al. Event-to-event intensification of the hydrologic cycle from 1.5 °C to a 2 °C warmer world. *Sci. Rep.* **9**, 3483 (2019).

182. Wiman, C., Hamilton, B., Dee, S. G. & Muñoz, S. E. Reduced lower Mississippi River discharge during the Medieval era. *Geophys. Res. Lett.* **48**, e2020GL091182 (2021).

183. Kettner, A. et al. Estimating change in flooding for the 21st Century under a conservative RCP forcing: a global hydrological modelling assessment. In *Global Flood Hazard: Applications in Modeling, Mapping, and Forecasting* AGU Geophysical Monograph Vol. 233 157–167 (Wiley-Blackwell, 2018).

184. McDonald, K. C., Kimball, J. S., Njoku, E., Zimmerman, R. & Zhao, M. Variability in springtime thaw in the terrestrial high latitudes: monitoring a major control on the biospheric assimilation of atmospheric CO_2 with spaceborne microwave remote sensing. *Earth Interact.* **8**, 1–23 (2004).

185. Cohen, S., Kettner, A. J. & Syvitski, J. P. M. Global suspended sediment and water discharge dynamics between 1960 and 2010: continental trends and intra-basin sensitivity. *Glob. Planet. Change* **115**, 44–58 (2014).

186. Bywater-Reyes, S., Segura, C. & Bladon, K. D. Geology and geomorphology control suspended sediment yield and modulate increases following timber harvest in temperate headwater streams. *J. Hydrol.* **548**, 754–769 (2017).

187. Tenorio, G. E. et al. Tracking spatial variation in river load from Andean highlands to inter-Andean valleys. *Geomorphology* **308**, 175–189 (2018).

188. Zeng, Z. et al. A reversal in global terrestrial stilling and its implications for wind energy production. *Nat. Clim. Change* **9**, 979–985 (2019).

189. Mirzabaev, A. et al. Desertification. In *Climate Change and Land: an IPCC Special Report on Climate Change, Desertification, Land Degradation, Sustainable Land Management, Food Security, and Greenhouse Gas Fluxes in Terrestrial Ecosystems* (eds Shukla, P. R. et al.) Ch. 3, 249–343 (IPCC, 2019).

190. Runeson, U. Forest fires — an overview. *Boreal Forests* http://www.borealforest.o.rg/world/innova/forest_fire.htm (2020).

191. Dennison, P. E., Brewer, S. C., Arnold, J. D. & Moritz, M. A. Large wildfire trends in the western United States, 1984–2011. *Geophys. Res. Lett.* **41**, 2928–2933 (2014).

192. Warrick, J. A. et al. The effects of wildfire on the sediment yield of a coastal California watershed. *GSA Bull.* **124**, 1130–1146 (2012).

193. DeBano, L. F. The role of fire and soil heating on water repellency in wildland environments: a review. *J. Hydrol.* **231–232**, 195–206 (2000).

194. Cannon, S. H. et al. Predicting the probability and volume of post-wildfire debris flows in the intermountain western United States. *Geol. Soc. Am. Bull.* **122**, 127–144 (2010).

195. Santi, P. M. & Ringers, F. K. Wildfire and landscape change. In *Treatise on Geomorphology* 262–287 (Elsevier, 2020).

196. DiBiase, R. A. & Lamb, M. P. Vegetation and wildfire controls on sediment yield in bedrock landscapes. *Geophys. Res. Lett.* **40**, 1093–1097 (2013).

197. DiBiase, R. A. & Lamb, M. P. Dry sediment loading of headwater channels fuels post-wildfire debris flows in bedrock landscapes. *Geology* **48**, 189–193 (2019).

198. Moody, J. A. & Martin, D. A. Synthesis of sediment yields after wildland fire in different rainfall regimes in the western United States. *Int. J. Wildland Fire* **18**, 96–115 (2009).

199. Neukom, R. et al. No evidence for globally coherent warm and cold periods over the preindustrial Common Era. *Nature* **571**, 550–554 (2019).

200. Hooijer, H. & Vernimmen, R. Global LiDAR land elevation data reveal greatest sea-level rise vulnerability in the tropics. *Nature. Nat. Commun.* **12**, 3592 (2021).

201. Syvitski, J. P. M. & Saito, Y. Morphodynamics of deltas under the influence of humans. *Glob. Planet. Changes* **57**, 261–282 (2007).

202. Syvitski, J. P. M. et al. Sinking deltas due to human activities. *Nat. Geosci.* **2**, 681–689 (2009).

203. Tessler, Z. et al. Profiling risk and sustainability in coastal deltas of the world. *Science* **349**, 638–643 (2015).

204. Giosan, L., Syvitski, J., Constantinescu, S. & Day, J. Climate change: protect the world's deltas. *Nature* **516**, 31–33 (2014).

205. Tessler, Z. D., Vörösmarty, C. J., Overeem, I. & Syvitski, J. P. M. A model of water and sediment balance as determinants of relative sea level rise in contemporary and future deltas. *Geomorphology* **305**, 209–220 (2018).

206. Minderhoud, P. S. J., Coumou, L., Erkens, G., Middelkoop, H. & Stouthamer, E. Mekong deltas much lower than previously assumed in sea-level rise impact assessments. *Nat. Commun.* **10**, 3847 (2019).

207. Kulp, S. A. & Strauss, B. H. New elevation data triple estimates of global vulnerability to sea-level rise and coastal flooding. *Nat. Commun.* **10**, 4844 (2019).

208. Ishitsuka, K. et al. Natural surface rebound of the Bangkok plain and aquifer characterization by persistent scatterer interferometry. *Geochem. Geophys. Geosyst.* **15**, 965–974 (2014).

209. Turner, R. E., Swenson, E. M., Milan, C. S. & Lee, J. M. Hurricane signals in salt marsh sediments: Inorganic sources and soil volume. *Limnol. Oceanogr.* **52**, 1231–1238 (2007).

210. Turner, R. E., Baustian, J. J., Swenson, E. M. & Spicer, J. S. Wetland sedimentation from hurricanes Katrina and Rita. *Science* **314**, 449–452 (2006).

211. Rogers, K. G., Syvitski, J. P. M., Overeem, I., Higgins, S. & Gilligan, J. Farming practices and anthropogenic delta dynamics. In *Proceedings IAHS-IAPSO-IASPEI Joint 37th Scientific Assembly, Gothenburg, Sweden* Vol. 358 133–142 (IAHS, 2013).

212. Wang, H. J. et al. Impacts of the dam-orientated water-sediment regulation scheme on the lower reaches and delta of the Yellow River (Huanghe): a review. *Glob. Planet. Change* **157**, 93–113 (2017).

213. Vousdoukas, M. I. et al. Economic motivation for raising coastal flood defenses in Europe. *Nat. Commun.* **11**, 2119 (2020).

214. Luijendijk, A. et al. The state of the world's beaches. *Sci. Rep.* **8**, 6641 (2018).

215. Mentaschi, L., Vousdoukas, M. I., Pekel, J.-F., Voukouvalas, E. & Feyen, L. Global long-term observations of coastal erosion and accretion. *Sci. Rep.* **8**, 12876 (2018).

216. Peduzzi, P. Sand, rarer than one thinks. *Environ. Dev.* **11**, 208–218 (2014).

217. Webb, A. Technical Report — an assessment of coastal processes, impacts, erosion mitigation options and beach mining (Bairiki/Nanikai causeway, Tungaru Central Hospital coastline and Bonriki runway — South Tarawa, Kiribati). EU-SOPAC Project Report Vol.46 (EU-SOPAC, 2005).

218. McKenzie, E., Woodruff, A. & McClennen, C. Economic assessment of the true costs of aggregate mining in Majuro atoll, Republic Of The Marshall Islands (South Pacific Applied Geoscience Commission (SOPAC), 2006).

219. De Schipper, M. A., Ludka, B. C., Raubenheimer, B., Luijendijk, A. P. & Schlaucher, T. A. Beach nourishment has complex implications for the future of sandy shores. *Nat. Rev. Earth Environ.* **2**, 70–84 (2021).

220. Syvitski, J. P. M. Supply and flux of sediment along hydrological pathways: research for the 21st century. *Glob. Planet. Change* **39**, 1–11 (2003).

221. Warrick, J. A. & Milliman, J. D. Hyperpycnal sediment discharge from semiarid southern California rivers: implications for coastal sediment budgets. *Geology* **31**, 781–784 (2003).

222. Milliman, J. D., Farnsworth, K. L., Jones, P. D., Xu, K. H. & Smith, L. C. Climatic and anthropogenic factors affecting river discharge to the global ocean, 1951–2000. *Glob. Planet. Change* **62**, 187–194 (2008).

223. National Oceanic and Atmospheric Administration (NOAA). NOAA delivers new U.S. climate normals: decadal update from NCEI gives forecasters and public latest averages for 1991–2020. *NOAA* https://www.ncei.noaa.gov/news/noaa-delivers-new-us-climate-normals (2021).

224. Brakenridge, G. R. et al. Calibration of satellite measurements of river discharge using a global hydrology model. *J. Hydrol.* **475**, 123–136 (2013).

225. Hudson, B. et al. MODIS observed increase in duration and spatial extent of sediment plumes in Greenland fjords. *Cryosphere* **8**, 1161–1176 (2014).

226. Dethier, E. N., Renshaw, C. E. & Magilligan, F. J. Toward improved accuracy of remote sensing approaches for quantifying suspended sediment: Implications for suspended-sediment monitoring. *J. Geophys. Res. Earth Surf.* **125**, e2019JF005033 (2020).

227. Brakenridge, G. R. et al. Design with nature: causation and avoidance of catastrophic flooding, Myanmar. *Earth Sci. Rev.* **165**, 81–109 (2017).

228. Verburg, P. H. et al. Methods and approaches to modelling the Anthropocene. *Glob. Environ. Change* **39**, 328–340 (2016).

229. Moragoda, N. & Cohen, S. Climate-induced trends in global riverine water discharge and suspended sediment dynamics in the 21st century. *Glob. Planet. Change* **191**, 103199 (2020).

230. Dunn, F. E. et al. Projections of declining fluvial sediment delivery to major deltas worldwide in response to climate change and anthropogenic stress. *Environ. Res. Lett.* **14**, 084034 (2019).

231. VEMAP Members. Vegetation/ecosystem modeling and analysis project: comparing biogeography and biogeochemistry models in a continental-scale study of terrestrial ecosystem responses to climate change and CO_2 doubling. *Glob. Biogeochem. Cycles* **9**, 407–437 (1995).

232. Warszawski, L. et al. The Inter-Sectoral Impact Model Intercomparison Project (ISI–MIP): project framework. *Proc. Natl Acad. Sci.* **111**, 3228–3232 (2014).

233. Tucker, G. E. et al. CSDMS: A community platform for numerical modeling of Earth-surface processes. *Geosci. Model Dev. Discuss.* https://doi.org/10.5194/gmd-2021-223 (2021).

234. Rousseau, Y., Watson, R. A., Blanchard, J. L. & Fulton, E. A. Evolution of global marine fishing fleets and the response of fished resources. *Proc. Natl Acad. Sci. USA* **116**, 12238–12243 (2019).

235. Nageswara Rao, K. et al. Palaeogeography and evolution of the Godavari delta, east coast of India during the Holocene: An example of wave-dominated and fan-delta settings. *Palaeogeogr. Palaeoclimatol. Palaeoecol.* **440**, 213–233 (2015).

236. Tanabe, S., Saito, Y., Vu, Q. L., Hanebuth, T. J. J. & Ngo, Q. L. Holocene evolution of the Song Hong (Red River) delta system, northern Vietnam. *Sediment. Geol.* **187**, 29–61 (2006).

237. Pithan, F. & Mauritsen, T. Arctic amplification dominated by temperature feedbacks in contemporary climate models. *Nat. Geosci.* **7**, 181–184 (2014).